https://doi.org/10.5194/tc-2021-73
Preprint. Discussion started: 25 March 2021

The Cryosphere Discussions

Elements of future snowpack modeling - part 2: A modular and extendable Eulerian–Lagrangian numerical scheme for coupled transport, phase changes and settling processes

Anna Simson[1], Henning Löwe[2], and Julia Kowalski[1,3]

[1]AICES Graduate School, RWTH Aachen University, Schinkelstr. 2a, 52062 Aachen, Germany
[2]WSL Institute for Snow and Avalanche Research SLF, Flüelastr. 11, 7260 Davos, Switzerland
[3]Computational Geoscience, Geoscience Centre of the University of Göttingen, Goldschmidtstr. 1, 37077 Göttingen, Germany

Correspondence: Anna Simson (simson@aices.rwth-aachen.de)

Abstract. A coupled treatment of transport processes, phase changes and mechanical settling is the core of any detailed snowpack model. A key concept underlying the majority of models is the notion of layers as deforming material elements that carry the information on their physical state. Thereby an explicit numerical solution of the ice mass continuity equation can be circumvented, however at the downside of virtual no flexibility in implementing different coupling schemes for densification, phase changes and transport. As a remedy we consistently recast the numerical core of a snowpack model into an extendable Eulerian–Lagrangian framework for solving the coupled non-linear processes. In the proposed scheme, we explicitly solve the most general form of the ice mass balance using the method of characteristics, a Lagrangian method. The underlying coordinate transformation is employed to state a finite-difference formulation for the superimposed (vapor and heat) transport equations which are treated in their Eulerian form on a moving, spatially non-uniform grid that includes the snow surface as a free upper boundary. This formulation allows to unify the different existing view points of densification in snow or firn models in a flexible way and yields a stable coupling of the advection-dominated mechanical settling with the remaining equations. The flexibility of the scheme is demonstrated within several numerical experiments using a modular solver strategy. We focus on emerging heterogeneities in (two-layer) snowpacks, the coupling of (solid-vapor) phase changes with settling at layer interfaces and the impact of switching to a non-linear mechanical constitutive law. Lastly, we discuss the potential of the scheme for extensions like a dynamical equation for the surface mass balance or the coupling to liquid water flow.

1 Introduction

The snow density is probably the most important prognostic variable of any snowpack model as e.g. reflected by a focus on snow water equivalent in past snow model intercomparison projects (Krinner et al., 2018, and references therein). That said, it actually comes as a surprise when not even the detailed snowpack models explicitly state an ice mass conservation

https://doi.org/10.5194/tc-2021-73
Preprint. Discussion started: 25 March 2021

equation in their technical documentation (Brun et al., 1989, 1992; Lehning et al., 2002; Bartelt and Lehning, 2002). Only a more detailed inspection reveals how mass conservation is accounted for, namely rather indirectly by stating a settling law for individual layers and resorting to a "Lagrangian coordinate system that moves with the ice matrix" (Bartelt and Lehning, 2002) to translate the ice phase deformation into a thickness evolution of the layers (Brun et al., 1989; Vionnet et al., 2012). While this procedure is well established for a long time, it is without numerical ambiguities only in the absence of phase changes. In addition, this non-explicit nature of the most important conservation law in snow makes it virtually impossible to isolate and advance the numerical core of a snowpack model as an encapsulated numerical scheme comprising all involved coupled non-linear partial differential equations.

This non-explicit treatment of snow density or ice mass continuity in snowpack models has to be contrasted to other existing work on densification, comprising both, stand-alone numerical snow studies (Meyer et al., 2020) and the vast body of work on firn densification (Lundin et al., 2017). All of the latter models are built around an explicit formulation of the ice mass continuity equation. This conceptual difference renders a general comparison of firn and snow densification mechanisms (Lundin et al., 2017) difficult. For model intercomparisons in the future it is thus desirable to have a numerical core that is able to digest arbitrary snow or firn densification physics, with a flexible but rigorous coupling to superimposed non-linear transport and phase change processes.

Any holistic snowpack model has to account for transport of heat, vapor and liquid water, its induced phase change processes, as well as mechanical settling and apparent metamorphic processes on the snow's microstructure. A widespread body of literature exists that proposes different modeling approaches and computational tools for the various flavors and perspectives of this multi-physics coupled situation, e.g. Krinner et al. (2018, and references therein). For the general timescales of interest (diurnal up to seasonal), it is common practice to employ a continuum assumption and to model the snowpack's state as a mixture of ice, vapor, water and air, as initially described in Bader and Weilenmann (1992). Detailed snowpack models, such as SNOWPACK (Lehning et al., 2002) and CROCUS (Vionnet et al., 2012) are built upon this type of mixture theoretical approach and used for a wide range of purposes.

While heat transport, mechanical settling and processes due to the presence of liquid water have been incorporated into SNOWPACK (Bartelt and Lehning, 2002) and CROCUS (Vionnet et al., 2012) for a long time, effects due to vapor transport have mostly recently been investigated in separate studies. Upscaled and homogenized continuum mechanical process models that account for vapor transport are, for instance, put forward by Hansen and Foslien (2015) and Calonne et al. (2014). Both couple the snowpack's evolving temperature profiles to a non-linear reaction-diffusion type of equation for vapor transport and phase change. While they provide different flavors of how to set up the underlying mathematical model, both approaches are formulated for idealized conditions and investigate vapor diffusion in the absence of settling and therefore neglect its feedback on the apparent snow density. These model-based investigations, but also field-based observations in arctic snowpacks on top of permafrost (Domine et al., 2016, 2019) demonstrated the significance of vapor related processes in snow. Hence, it is of great interest to investigate further, how vapor interacts with apparent mechanical processes within the snowpack.

Incorporating vapor transport directly into a fully coupled snowpack model is however challenging, e.g. due to the fact that the associated characteristic time scales are small, and expected effects on the snowpack are localized (Schürholt et al., 2020).

https://doi.org/10.5194/tc-2021-73
Preprint. Discussion started: 25 March 2021

Both requires a much higher spatio-temporal resolution than typically provided by existing operational schemes. In its original version, SNOWPACK for instance uses time steps in the order of 15 min or larger to facilitate seasonal simulation times. The recent work of Jafari et al. (2020) provides a first attempt to account for vapor transport within a coupled snowpack model. In their paper, they accounted for diffusive vapor transport and phase change following Hansen and Foslien (2015) and analyzed its feedback on the snow density. In order to resolve diffusive processes, simulations were conducted at much shorter time steps of 1 min and a finer spatial resolution at approximately 0.1 cm. While this work demonstrates the general feasibility of vapor-coupled snowpack models, the exact nature of how vapor transport and phase changes interfere with stress-induced settling remains to be investigated in-depth.

It is well known that any numerical strategy that aims at simulating simultaneous settling-induced deformation of the snowpack and (arbitrary) diffusive transport requires a special computational treatment to couple both. Diffusive transport and reactive phase change is best modelled by taking a Eulerian perspective, hence on a static mesh. In contrast there exist a number of different techniques to incorporate the settling induced deformation. One option is to use a time-dependant coordinate transformation by Morland (1982), who developed a fixed domain transformation to solve one-phase diffusion problems with a moving free surface on a finite, time-invariant computational domain. An alternative approach was put forward by Wingham (2000), who used a different spatio-temporal coordinate transformation for firn densification. Both transformation strategies effectively eliminate the vertical motion (or gradients of it) from the computational update procedure. And exactly the same is (implicitly) done in the present treatment of densification in snowpack models, where the coordinate transformation embodied in deformation of the underlying computational grid through the update of layer positions/thicknesses is (implicitly) exploited for the ice mass conservation. However, the present descriptions do not take the full advantage of a clear and explicit separation into a Lagrangian deformation module that accounts for mechanical settling and a Eulerian transport and phase change module. The benefit of this hybrid computational strategy is that it is easy to understand, computationally feasible, provides a modular error control and increases the interpretability by disentangling numerical artefacts from features of the underlying non-linear process models. Hybrid numerical schemes that combine an Eulerian process model with a Lagrangian-type spatio-temporal mesh adaptation are not new and have been used in other disciplines, e.g. for phase change problems (Lacroix and Garon, 1992), as σ-coordinates in oceanography (Mellor and Blumberg, 1985), or for shallow flow models (Kowalski and Torrilhon, 2019).

The aim of our work is twofold: First, we will describe our numerical strategy for a phase-changing snowpack. The numerical scheme is hybrid, in the sense that it clearly discriminates between a solution of the mechanical settling operator by means of a Lagrangian approach and a solution to the transport and phase change operator by means of an Eulerian approach. To some degree, the numerical model description must be understood as a rigorous re-formulation of the numerical schemes from existing computational snowpack models. Yet, in addition to existing schemes we a) explicitly separate the Eulerian and Lagrangian part of the solver to facilitate a later modular adaption, b) provide a full finite difference formulation including correction terms due to the deforming (non-uniform) mesh that are typically omitted and c) discuss options to increase the approximation accuracy of the various parts of the numerical scheme. Second, we demonstrate the computational potential by applying and analyzing simulation results for an idealized two-layer, dry snow situation. We consider a model cascade

https://doi.org/10.5194/tc-2021-73
Preprint. Discussion started: 25 March 2021

of different process building blocks, which in their most comprehensive version, correspond to fully coupled heat and vapor transport alongside phase changes and settling.

With this work we seek to contribute to anticipated future developments of snow or firn models, or likewise extensions of existing ones, that aim at flexibility and modularity, while providing a simple, mathematically rigorous numerical approximation for a stable and robust integration of generic multi-physics process equations. By modularity and extendability we understand the possibility to consider or neglect specific process modules and parametrizations in a straight-forward way. This modularity would enable to a) investigate competing non-linear effects systematically from a cascade of process models, b) assess the quality of the numerical approximation independently and c) conduct a standardized model selection based on well-defined benchmarks.

The article is structured as follows. In Sect. 2, we recall the dry snow model equations comprising the relevant transport, phase change and mechanical aspects. In Sect. 3, we introduce the Eulerian-Lagrangian numerical scheme and its solution using the method of characteristics. In Sect. 4, we present and discuss results from a number of simulation scenarios, including verification scenarios that consider transport, phase changes, and mechanics in the absence of any interaction, as well as coupled scenarios that focus on their interplay. We furthermore investigate the impact of different viscosity parametrizations and assess the behavior when switching to a Glen-type of non-linear constitutive closure. Finally, we compare our results to a conventional layer-based treatment. In Sect. 5, we summarize and discuss our findings, and draw conclusions towards future snowpack modeling.

2 Physical model

2.1 General situation

As a common starting point, snow models take a macroscale perspective that volume-averages or homogenizes the snowpack's microstructural state into macroscale variables. If not stated otherwise, we implicitly assume all state variables to be macroscale variables without explicitly mentioning it every time. State variables, model parameters and constants used in this paper are summarized in Table 1.

The amount of ice within one reference volume is referred to the ice volume fraction ϕ_i which for dry snow is related to the snow density by $\phi_i \rho_i$ with ρ_i ice density. In a general snowpack, the ice matrix's void space $1 - \phi_i$ is filled to different degrees with air, vapor, or even water. Structure and volume fraction of the ice can change over time either due to strain-induced settling processes, or due to transient phase changes, such as sublimation and deposition or melting and freezing. Our study focuses on the derivation of a hybrid Eulerian-Lagrangian framework to solve settling, transport and phase changes with an assessment of the computational building blocks. To this end we restrict ourselves to dry snow and allow for one secondary phase (vapor) in a Eulerian treatment coupled to the Lagrangian treatment of the ice phase. With respect to computational model development, we regard the dry snow situation as the more challenging (yet less investigated) one, mostly due to a broader spectrum of characteristic spatial and temporal scales involved. Note, that water transport and solid-liquid phase change can in principle

https://doi.org/10.5194/tc-2021-73
Preprint. Discussion started: 25 March 2021


The Cryosphere Discussions
Open Access
EGU

be integrated following a similar strategy presented in this paper. The following section introduces the (macroscale) snowpack model where the subsection structure reflects the later described modular structure of the numerical core.

Table 1. Terminology of state variables, model parameters and constants

Symbol	Name	Equation/Value	Unit
State variables			
T	Temperature	Eq. (11)	K
ϕ_i	Ice volume fraction	Eq. (1)	$-$
c	Ice deposition rate	Eq. (9)	kg m^{-3} s^{-1}
ρ_v	Vapor density	Eq. (A1)	kg m^{-3}
v	Vertical velocity	Eq. (7)	m s^{-1}
Effective model parameters of snow			
ρ_{eff}	Density		kg m^{-3}
$(\rho C)_{eff}$	Heat capacity	Eq. (A4)	J m^{-3} K^{-1}
D_{eff}	Vapor diffusion coefficient	Eq. (A2)	m^2 s^{-1}
k_{eff}	Thermal conductivity	Eq. (A3)	W m^{-1} K^{-1}
Parameters assumed to be constant (Calonne et al., 2014)			
ρ_i	Ice density ϕ_i = 1	917	kg m^{-3}
k_i	Ice thermal conductivity ϕ_i = 1	2.3	W m^{-1} K^{-1}
k_a	Air thermal conductivity ϕ_i = 0	0.024	W m^{-1} K^{-1}
C_i	Ice heat capacity ϕ_i = 1	2000	J kg^{-1} K^{-1}
C_a	Air heat capacity ϕ_i = 0	1005	J kg^{-1} K^{-1}
L	Ice latent heat of sublimation	2835332.6	J kg^{-1}

2.2 Ice mass balance

The ice volume fraction $\phi_i = \phi_i(\mathbf{z}, t)$ within a spatio-temporally evolving snowpack of varying snow height $H(t)$ is governed by the ice mass balance and reads

$$\partial_t \phi_i + \nabla \cdot (\mathbf{v}\, \phi_i) = \frac{c}{\rho_i}, \tag{1}$$

with velocity field $\mathbf{v}$, source term c, and intrinsic ice density ρ_i.

In a 1d situation that focuses on an evolving vertical snow column, we have vertical position z as the only relevant spatial coordinate ($z \in [0, H(t)]$). The velocity field $\mathbf{v}$ reduces to vertical velocity $v = v(z, t)$ that depends on time and position within the column. It is negative for snow height decrease and positive for snow height increase. Vertical motion results either from mechanical settling, hence a consolidation or compaction of the snowpack, or alternatively it is a continuity response to changes in ice volume from sublimation/deposition, which leads to a minor vertical decrease/increase of snow height. Though effects due to consolidation of snow may be significantly more pronounced than those due to phase change processes in the pore space,

https://doi.org/10.5194/tc-2021-73
Preprint. Discussion started: 25 March 2021

the latter needs to be accounted for to acknowledge mass conservation of the complete system. At this point in time, we do not consider any additional increases of snow height due to precipitation, yet we discuss how this can be included in the future in Sect. 5.

The source term $c = c(z,t)$ varies with time and position in the column and stands for a gain or loss of ice mass per unit volume and unit time. It is positive (production) if new ice is built, hence vapor deposits, and it is negative (loss) if ice is lost, hence sublimates. Henceforth we will refer to c as the deposition rate. Finally, ρ_i denotes the constant intrinsic density of ice and serves as a scaling factor. The ice mass balance (Eq. (1)) couples mechanical settling and phase change processes. Considering the equation in its full form is essential for our goal to model and eventually analyze the interplay between these processes. The structure of the ice mass balance resembles an advection-reaction equation that can conveniently be solved by means of Lagrangian type computational methods, such as the method of characteristics (see Sect. 3). Yet in order to do so, we need to provide a closure for both vertical velocity v and deposition rate c.

2.3 A closure for the velocity field

Velocity v represents mechanical deformation in the snowpack. Its idealized relation to the strain rate is given by

$$\nabla v = \dot{\epsilon}, \tag{2}$$

Note that this is simplified with respect to more general, tensorial formulations of 1d consolidation theories, see for instance Audet and Fowler (1992). Yet even the idealized formulation Eq. (2) will be sufficient for our purposes, as it resembles the approach typically chosen in snowpack models.

In general one would expect that porous snow inherits the non-linear constitutive behavior of ice (Kirchner et al., 2001), which leads to

$$\dot{\epsilon} = \frac{1}{\eta}\sigma^m, \tag{3}$$

which is a variant of Glen's law. Here, η denotes the compactive viscosity of snow and σ denotes the stress. The choice of the Glen exponent m in earlier work depends on both the physical regime but also on computational feasibility. The linear form of Glen's law ($m = 1$) is chosen in Vionnet et al. (2012) and Bartelt and Lehning (2002). For the sake of comparability we thus mainly use a linear version of Glen's law, hence $m = 1$. Our framework, however, also copes with the non-linear relation, such as $m = 3$, and we later include a comparative example.

The compactive viscosity η depends on the snow's microstructure and is challenging to be determined from experiments (Wiese and Schneebeli, 2017). It is typically provided as a parametrized closure for a specific physical situation and strongly correlates with the choice for the Glen exponent m. This fact clearly constrains its universal applicability and makes any transfer of a validated snowpack model to other physical situations challenging. In this article, we will consider both constant viscosity scenarios, as well as an additional scenario with a varying viscosity assuming an empirical viscosity closure from Vionnet et al. (2012)

$$\eta(\phi_i, T) = f\,\eta_0\,\frac{\rho_i\,\phi_i}{c_\eta} exp\left(a_\eta\,(T_{ph} - T) + b_\eta\,\rho_i\,\phi_i\right), \tag{4}$$

https://doi.org/10.5194/tc-2021-73
Preprint. Discussion started: 25 March 2021


The Cryosphere Discussions
Open Access
EGU

with state variables temperature T and ice volume fraction ϕ_i and constants ice density ρ_i, phase change temperature $T_{ph} = 273$ K and further constants $\eta_0 = 7.62237 \times 10^6$ kg s^{-1}, $a_\eta = 0.1$ K^{-1}, $b_\eta = 0.023$ m^3 kg^{-1}, $c_\eta = 250$ kg m^{-2}. Finally, f reflects properties of the snow microstructure and is assumed to be 1 in our case. The constant viscosity value applied to linear Glen's law $\eta_{const,m=1}$ is derived with intermediate values for ice volume fraction and temperature of the respective initial conditions. These values are plugged into the empirical closure Eq. (4) to solve for viscosity. The same procedure cannot be applied to derive a constant viscosity value for the non-linear version of Glen's law $\eta_{const,m=3}$ since the viscosity closure (Eq. (4)) has initially been calibrated to the linear form of Glen's law ($m = 1$). Instead we choose a snow deformation rate from the literature ($\dot{\epsilon} = 10^{-6}$ s^{-1} (Johnson, 2011)) and determine the maximum stress value from the initial snow density. These strain rate and stress values are then inserted into the constitutive relation (Eq. (3)) which is finally solved for viscosity. To avoid infinite ice volume growth above physical values ($\phi_i > 1$) the viscosity must tend to infinity for $\phi_i \to 1$. Therefore, the constant viscosity values are restricted to ice volumes below 0.95 by multiplication with an ice volume fraction dependent power law (Appendix (A6)). This power law yields ≈ 1 for $\phi_i \leq 0.95$ and exponentially increases for higher ice volumes. Multiplied with the constant viscosity values viscosity remains constant below $\phi_i < 0.95$ and exponentially increases above, which stops further densification and settling. This procedure does not intend to reproduce the correct physics for low porosity ice, which mathematically leads though to a similar crossover behavior.

In the absence of strong horizontal deformation and deviatoric stress components, it is reasonable to assume a stress-free condition at the snow's surface and a hydrostatic stress condition in its interior:

$$\nabla \sigma = g\, \rho_{eff}. \tag{5}$$

Here, ρ_{eff} refers to the snowpack's effective density, which is clearly dominated by the ice fraction via $\rho_{eff} \approx \phi_i(z)\, \rho_i$. It varies with the position z in the snow column due to a vertically varying ice volume fraction $\phi_i(z)$. Integration of Eq. (5) and combination with Eqs. (2) and (3) yields an expression for the velocity gradient:

$$\partial_z v = \frac{1}{\eta} \left(g \int_z^{H(t)} \phi_i\,(\zeta)\, \rho_i\, d\zeta \right)^m . \tag{6}$$

A second integration along the vertical axis finally yields an expression for the velocity at position z in the snow column:

$$v(z) = -\int_0^z \frac{1}{\eta} \left(g \int_{\tilde{z}}^{H(t)} \phi_i(\zeta) \rho_i d\zeta \right)^m d\tilde{z}, \tag{7}$$

in terms of total height $H(t)$, ice volume fraction $\phi_i(z,t)$, and with $v(z=0,t) \equiv 0$. This definition of the vertical velocity yields a process that complies with the obvious physical constraints: a) the velocity vanishes at the bottom of the snow column, hence prevents artificial penetration into the ground. This is similar to displacement requirements in SNOWPACK (Bartelt and Lehning, 2002). b) the vertical velocity accumulates with height, which prevents any artificial disaggregation of the snowpack, and c) the vertical velocity relaxes towards zero as the ice volume fraction tends towards its maximum volume fraction $\phi_i < \phi_{i,max} < 1$. In the ongoing of this paper, we will use Eq. (7) to account for the mechanical settling of the snowpack.

https://doi.org/10.5194/tc-2021-73
Preprint. Discussion started: 25 March 2021


The Cryosphere Discussions

2.4 Transport and phase changes

The ice deposition rate c as relevant to solve Eq. (1) typically depends on a cascade of coupled heat and mass transport for the involved phases ice, water and vapor. In this article, we will consider a process model proposed by Hansen and Foslien (2015) that reflects a dry snow condition in which void space is filled by vapor only. Note, however, that this coupled process model could readily be substituted or extended by another one, e.g. the one from Calonne et al. (2014).

Next, we state the essential aspects and process equations of the model proposed in Hansen and Foslien (2015). We extend the model for mechanics and describe how it can be used to recover the ice deposition rate:

Assuming dry snow conditions, the ice production is solely determined by mass transport between vapor and ice. The vapor mass balance reads

$$\partial_t \left(\rho_v \left(1-\phi_i\right)\right) - \nabla \cdot \left(D_{eff}\, \nabla \rho_v\right) + \rho_v\, \nabla \cdot \left(v\, \phi_i\right) = -c, \tag{8}$$

in which ρ_v denotes the vapor density and D_{eff} the effective vapor diffusion coefficient. Note that the convective term on the left hand side derives from mechanical settling and is thus not included in Hansen and Foslien (2015). Its effect on deposition rate is rather low, and thus it is neglected in the following. Vapor production corresponds to negative ice deposition rate $-c$ that represents sublimation. Following Hansen and Foslien (2015), vapor density in the pore space can be assumed to be at saturation density ρ_v^{eq}, so that $\rho_v \equiv \rho_v^{eq}$. The latter is well investigated, and empirical relations exist that specify its temperature dependency $\rho_v^{eq}(T)$. In this work, we will employ an empirical relation from Libbrecht (1999). The full expression can be read in Appendix A1. Instead of following the approach of Hansen and Foslien (2015) one could also use another closure for the source term (Calonne et al., 2014; Jafari et al., 2020; Schürholt et al., 2020). Due to the closure for vapor density ρ_v, the vapor mass balance (Eq. (8)) can be rewritten using the temperature dependence of the equilibrium vapor density

$$\left(1-\phi_i\right) \frac{d\rho_v}{dT}\, \partial_t T - \nabla \cdot \left(D_{eff}\, \frac{d\rho_v}{dT}\, \nabla T\right) = -c. \tag{9}$$

Assuming the snow to be in thermal equilibrium at the microscale, we can likewise write the energy balance in terms of the temperature, which reads

$$\left(\rho C\right)_{eff}\, \partial_t T - \nabla \cdot \left(k_{eff}\, \nabla T\right) = c\, L. \tag{10}$$

The parameters $(\rho C)_{eff}$ and k_{eff} stand for the effective heat capacity of snow and effective thermal conductivity, respectively. Both parameters depend on the ice volume fraction, and their definition is stated in Appendix A2. The right hand side of the heat equation accounts for latent heat release, which is coupled to phase change processes.

The system of the two equations, Eqs. (9) and (10), and the two unknowns, temperature T and deposition rate c, is solved by replacing c in Eq. (10) with Eq. (9), which yields a non-linear equation for temperature

$$\left(\left(\rho C\right)_{eff} + \left(1-\phi_i\right) \frac{d\rho_v(T)}{dT}\, L\right) \partial_t T = \nabla \cdot \left(\left(L\, D_{eff}\, \frac{d\rho_v(T)}{dT} + k_{eff}\right) \nabla T\right). \tag{11}$$

The spatio-temporal temperature evolution is then used to recover the ice deposition rate c from either Eq. (9) or Eq. (10).

https://doi.org/10.5194/tc-2021-73
Preprint. Discussion started: 25 March 2021

3 Computational Approach

The complete process model is now given by the ice mass balance Eq. (1), its mechanically induced vertical velocity Eq. (7), and the coupled system for temperature Eq. (11) and ice deposition rate determined by either Eq. (9) or Eq. (10). Each of the equations will be solved in a separate module. The ice mass balance in conjunction with the vertical velocity has the form of a non-linear advection equation, whereas the remaining equations are of parabolic nature, which is reflected in our general approach to solve the system.

3.1 General approach to the computational strategy

Based on the distinction into diffusion and advection dominated processes, we propose a two-step solution scheme:

Step 1 accounts for the mesh deformation and solves the advection dominated mechanical settling, i.e. the ice mass balance Eq. (1), by means of a Lagrangian approach, and

Step 2 determines the spatio-temporal evolution of temperature and deposition rate fields as introduced in Sect. 2.4 based on an Eulerian approach that solves the diffusion dominated transport and phase changes via a finite difference implementation on a deformed (unstructured) mesh.

Note that here, we employed a finite difference method because it provides a feasible algorithm that results at the necessary accuracy for the scenarios considered in the paper. It also naturally integrates with the Lagrangian part of the solution (Step 1), as we can re-use the same mesh. In principle, it is also possible to couple the two-step approach with a finite element solution for temperature and deposition rate, e.g. when aiming for a 2d or 3d model in a complex geometry. In that situation, however, we have to keep in mind that deposition rate and temperature fields need to be reconstructed from a finite element solution at each time step. Especially when wanting to use higher order elements this might limit computational feasibility.
Our solution scheme alternates both steps via straightforward first order operator splitting. This is found to work well for our simulation scenarios, yet could be readily exchanged with a higher order splitting scheme, e.g. a second order Strang splitting, if required.
The computational model is implemented into Python and it is modular and extendable, in the sense that each module can separately be activated and deactivated. This not only simplifies the verification of individual process building blocks, yet also allows an in-depth investigation of the various coupling effects and the model's non-linear feedback. Alternative formulations e.g. of the parametrized velocity field are implemented and can easily be exchanged. Finally, the modular structure facilitates the implementation of additional closure relations or the integration of entire new process modules.

https://doi.org/10.5194/tc-2021-73
Preprint. Discussion started: 25 March 2021

3.2 Computational grid

In this study, we consider a 1d snow column, which is discretized into $nz+1$ spatial mesh nodes denoted by z_k with $k \in \{0,1,..,nz\}$. We applied 101 computational nodes ($nz = 100$) except for some simulations that required a higher resolution of 251 nodes ($nz = 250$). The mesh is non-uniform in general, meaning that the distance between neighboring nodes $z_{k+1} - z_k$ varies throughout the snow column and with time. Note that the axis is oriented opposing gravitational acceleration, such that z_0 denotes the position of the ground and z_{nz} the position of the snowpack's free surface. Time increments are denoted by t_n with $n \in \{0,1,..,nt\}$ and nt being the maximum number of time steps in a complete simulation run. For each of the field variables subscript k denotes the vertical coordinate and superscript n denotes the time step hence $T(z_k, t_n) = T_k^n$.

3.3 Lagrangian solution of the ice mass balance

When the snowpack is subject to vertical motion, e.g. settling, its physical height decreases, hence its vertical extent shrinks. One option to reflect this in a computational method is to adjust the spatial node coordinates accordingly. The challenging fact in our situation is that the vertical motion within the snow column (non-linear advection) is coupled to phase changes, i.e. a change in ice volume fraction via the source term in the ice mass balance (Eq. (1)). The method of characteristics is a suitable method to solve such a non-linear advection equation with source term. It can be interpreted as a simultaneous motion tracking of snow material elements or "particles", referred to as the integration along so-called characteristics, while also accounting for its metamorphism along the trajectory. By construction, the method correctly tracks the snowpack's moving free surface. Due to the fact that the snow column's evolution is determined with respect to a material particle that moves vertically at speed v in the snowpack, the method of characteristics is called a Lagrangian approach.

In order to derive the specific update rule for the ice mass balance Eq. (1), we first apply the chain rule to its initial Eulerian version

$$\partial_t \phi_i + v\, \partial_z \phi_i = \frac{1}{\rho_i} c - \partial_z v\, \phi_i \tag{12}$$

and then re-formulate the equation in a Lagrangian reference frame, hence with respect to nodes moving at the vertical velocity v. Changing to the moving reference frame effectively compensates the advection term in Eq. (12) and yields

$$\partial_t \phi_i = \frac{1}{\rho_i} c + \partial_z v\, \phi_i \tag{13}$$

$$\partial_t z = v. \tag{14}$$

Equation (14) accounts for the settling of material particles within the snowpack. We will use it to update the coordinates of the mesh nodes directly, which results in a continuous mesh deformation as illustrated in Fig. 1. Equation (13) captures the evolution of the ice volume fraction along the trajectory of a moving ice material particle within the snowpack. It accounts for volume changes due to a) mass production/loss in response to phase changes, and b) vertical variation of the vertical velocity. Further details and generalizations of the method of characteristics can be found in Farlow (1993).

Equations (13) and (14) can be solved analytically for a constant vertical velocity and deposition rate. In our case however, the

https://doi.org/10.5194/tc-2021-73
Preprint. Discussion started: 25 March 2021

velocity closure is provided by Eq. (7) and the deposition rate results from solving yet another process model (Eqs. (10) and (11)), which requires a numerical solution. Since we expect the response of the ice volume fraction to be slow (with respect to other processes in the system), we will rely on a first order explicit Euler time integration scheme:

$$\phi_{i,k}^{n+1} = \phi_{i,k}^{n} + \Delta t \left(\frac{1}{\rho_i} c_k^n + \partial_z v_k^n \, \phi_{i,k}^n \right) \tag{15}$$

$$z_k^{n+1} = z_k^n + \Delta t \, v_k^n, \tag{16}$$

In order to update the mesh coordinates according to Eq. (16) for the vertical velocity closure derived before, we need to numerically approximate Eq. (7) at each node z_k, which results in

$$v(z_k) = \sum_{j=0}^{k} (\frac{1}{\eta} \sigma_j^m) \, \Delta z_j \tag{17}$$

with $\Delta z_j := z_j - z_{j-1}$, m Glen exponent, η viscosity and σ_j denoting the stress exerted by the overburdened snow mass

$$\sigma_j = \sum_{l=j}^{nz} g \, \phi_{i,l} \, \rho_i \, \Delta z_l. \tag{18}$$

with g gravitational acceleration. The forward Euler scheme of Eqs. (15) and (16) via the method of characteristics combined with the velocity update (Eq. (17)) essentially resembles the treatment of mass conservation as it is e.g. presently done in SNOWPACK. However, the explicit formulation and numerical treatment of Eqs. (15) and (16) allows to employ also other (e.g. higher order, implicit, etc.) solution schemes for both equations, if this was required to capture detailed aspects of the spatio-temporal coupling of phase changes (c) and settling (via $\partial_z v$) (cf. also the discussion in Sect. 5). To solve Eq. (15), we directly discretize the velocity's spatial derivative $\partial_z v$, which corresponds to the strain rate $\dot{\epsilon}_k^n = \frac{1}{\eta} \sigma_k^m$ given via Eq. (3). This is beneficial, as it avoids to numerically approximate the velocity gradient. The complete numerical update of ice volume fraction ϕ_i and mesh coordinates z can now concisely be written as

$$\phi_{i,k}^{n+1} = \phi_{i,k}^{n} + \Delta t \left(\frac{1}{\rho_i} c_k^n + \frac{1}{\eta} \left(\sum_{l=j}^{nz} g \, \phi_{i,l}^n \, \rho_i \Delta z_l^n \right)^m \phi_{i,k}^n \right) \tag{19}$$

$$z_k^{n+1} = z_k^n + \Delta t \left(\sum_{j=0}^{k} \frac{1}{\eta} \left(\sum_{l=j}^{nz} g \, \phi_{i,l}^n \, \rho_i \, \Delta z_l^n \right)^m \Delta z_j \right). \tag{20}$$

Similar to existing layer-based schemes, see for instance Sect. 3.4. in Bartelt and Lehning (2002) or its recent extension Jafari et al. (2020), the method of characteristics provides information on the settling of layers within the snowpack. Yet in addition, it serves as a basis for a fully modular and flexible computational strategy, that a) by construction accounts for the two-way feedback between the ice volume fraction and mass production or decay rates resulting from phase changes as a response to transport processes with in the snowpack, b) allows for a flexible adoption/extension of the process model (used to determine c) and the velocity closure. The latter could for instance serve as a pathway to integrate a data-driven velocity closure (or assimilation) from measurements. Such flexibility in numerical tools will be important in the future to

https://doi.org/10.5194/tc-2021-73
Preprint. Discussion started: 25 March 2021

conduct model comparisons, such as presented in Schürholt et al. (2020) within holistic snowpack models, or even a formalized Bayesian model selection that allows to infer on the most plausible process model out of a pool of candidate models given a certain data. A remaining difficulty now is to provide a (Eulerian) numerical scheme for diffusive processes that can operate on a spatially varying unstructured mesh.

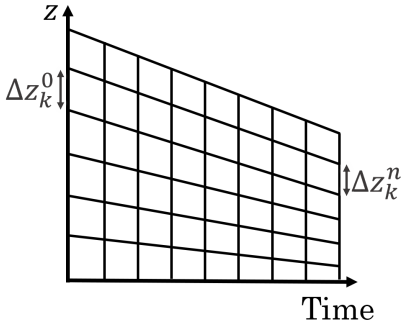

Figure 1. The snowpack height varies with time, e.g. shrinks due to settling of the snow. This has to be incorporated into the computational mesh, which undergoes deformation due to the downward movement of the free surface. The initially equidistant mesh does not uniformly change, which results into a mesh of varying node distances, so that in general $\Delta z_k^0 \neq \Delta z_k^n$.

3.4 Eulerian solution of transport and phase changes on a moving mesh

The process model accounting for heat transport Eqs. (9) and vapor transport (11) has to be solved with respect to a moving computational mesh according to Eq. (16). Both equations have the same generic structure, namely

$$\alpha\,\partial_T T - \partial_z\left(\beta\,\partial_z T\right) \tag{21}$$

with

$$\begin{aligned}
&\alpha = \alpha_T = (\rho C)_{eff} + (1-\phi_i)\,\frac{d\rho_v(T)}{dT} \quad \text{and} \quad \beta = \beta_T = L\,D_{eff}\,\frac{d\rho_v(T)}{dT} \text{ for heat equation Eq. (11), and} \\
&\alpha = \alpha_c = (1-\phi_i)\,\frac{d\rho_v(T)}{dT} \quad \text{and} \quad \beta = \beta_c = D_{eff}\,\frac{d\rho_v(T)}{dT} \quad \text{for vapor transport equation Eq. (9).}
\end{aligned} \tag{22}$$

An implicit first order finite difference approximation of Eqs. (9) and (11) for a spatially varying mesh of increments Δz_k^n results in

$$\alpha_{T,k}^n \frac{T_k^{n+1} - T_k^n}{\Delta t} = \frac{2\cdot\left(\beta_{T,k+1/2}\left(T_{k+1}^{n+1} - T_k^{n+1}\right) - \beta_{T,k-1/2}\left(T_k^{n+1} - T_{k-1}^{n+1}\right)\right)}{\left(\Delta z_k^n\right)^2 + \left(\Delta z_{k-1}\right)^2} - E_T(T_{k+1}^n, T_k^n, T_{k-1}^n) \tag{23}$$

$$\alpha_{c,k}^n \frac{T_k^{n+1} - T_k^n}{\Delta t} = \frac{2\cdot\left(\beta_{c,k+1/2}\left(T_{k+1}^{n+1} - T_k^{n+1}\right) - \beta_{c,k-1/2}\left(T_k^{n+1} - T_{k-1}^{n+1}\right)\right)}{\left(\Delta z_k^n\right)^2 + \left(\Delta z_{k-1}\right)^2} - c_k^{n+1} - E_c(T_{k+1}^n, T_k^n, T_{k-1}^n). \tag{24}$$

Note that parameters α_f and β_f for $f \in \{T, c\}$ also vary in space and time, and will be (explicitly) evaluated based on the snowpack's state at time n. $\beta_{f,k\pm1/2}$ accounts for the parameter's arithmetic mean between two neighboring cells. The terms

https://doi.org/10.5194/tc-2021-73
Preprint. Discussion started: 25 March 2021

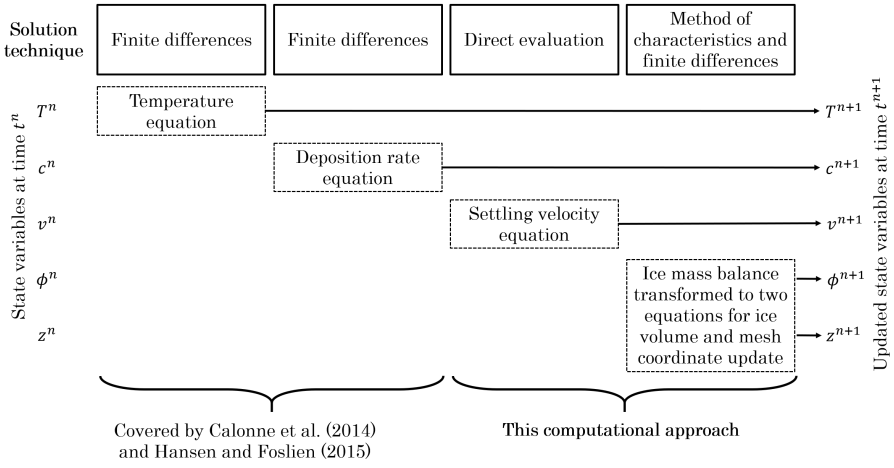

Figure 2. Illustrates the computational workflow of one iteration. The state variables at time t^n, depicted on the left hand side are updated through the modules annotated as dashed boxes, and ordered diagonally in the centre of the figure. After each update the state variables at time t^{n+1} are retrieved. The equations of the modules are implemented into the computational model through the respective solution technique stated in the solid boxes on the top row. The computational steps are carried out from top to bottom. The equations for heat and vapor transport have already been implemented by Calonne et al. (2014) and Hansen and Foslien (2015). A feedback on the ice volume fraction in the absence of a vertical velocity has been investigated in the companion paper (Schürholt et al., 2020). The modules for vertical velocity and for the coupled update of ice volume fraction and mesh coordinates, through the method of characteristics is novel in our approach.

E_c and E_T are error terms for the vapor and temperature equations, controlled by the temperature gradient. These error terms account for the necessary correction due to non-uniformity of the mesh and vanish for equidistant meshes. Their complete form is given in Appendix B, and their effect on the accuracy of the simulation is discussed in Sect. 4.4.

335 The complete numerical update can be concisely written in matrix form, which matches with the way it is implemented in the software

$$\boldsymbol{T}^{n+1} = \mathbf{A_T}^{-1} \left(\mathbf{B_T} \boldsymbol{T}^n + \mathbf{E}_T \boldsymbol{T}^n \right) \tag{25}$$

$$\boldsymbol{c}^{n+1} = \mathbf{A_c} \boldsymbol{T}^{n+1} + \mathbf{B_c} \boldsymbol{T}^n + \mathbf{E}_C \boldsymbol{T}^n. \tag{26}$$

First, Eq. (25) is solved for temperature T^{n+1}. Next, the updated temperature is used to solve Eq. (26) for the deposition 340 rate c^{n+1}. The complete matrix definitions are given in Appendix C. Note, that formally, it would be possible to add up matrices $\mathbf{B_T}$ and $\mathbf{E_T}$ as well as $\mathbf{B_c}$ and $\mathbf{E_c}$. We decided to keep them in this particular form to stress the similarity of this formulation with a standard finite difference approximation on an equidistant mesh, in which we are left with $\mathbf{B_T}$ and $\mathbf{B_c}$ and $\mathbf{E_T}$ and $\mathbf{E_c}$ vanish.

https://doi.org/10.5194/tc-2021-73
Preprint. Discussion started: 25 March 2021

3.5 Iterative coupling of Eulerian and Lagrangian solutions

The derived numerical update routines for temperature, deposition rate, vertical velocity and ice volume fraction comprise the four main modules that are sequentially called to update the respective state variables for one time step. A schematic illustration is given in Fig. 2. The time step size for the next time step $n+1$ is dynamically updated according to the mesh Fourier number based on the diffusivity $\frac{\beta_T}{\alpha_T}$ of heat of the current time step n

$$\Delta t^{n+1} = min(\frac{0.5\,\alpha_T^n\,(\Delta z^n)^2}{\beta_T^n}). \tag{27}$$

Since this choice for the time step computation did not yield instabilities, we excluded the vapor's diffusivity for the time step computation. The final iterative approach can be summarized as:

1. determine time step size Δt according to Eq. (27),
2. update the temperature field based on Eq. (23),
3. compute the deposition rate with the temperature field based on Eq. (24),
4. determine the vertical velocity with Eqs. (17) and (18), and
5. update the ice volume fraction and the mesh coordinates simultaneously based on Eqs. (19) and (20).

While 1.-3. is a re-implementation of an existing approach previously published by (Hansen and Foslien, 2015; Calonne et al., 2014), their coupling to 4. and 5. constitutes the novelties of our work, see also Fig. 2. Note that 4. is computed as part of 5. in the code. Our implementation is modular in the sense that it allows for a coupling with other process models that comply with a non-uniform mesh. In the following results (Sect. 4) this modularity is used to asses the individual effect of the different process building blocks by a strategical activation and deactivation of the modules.

4 Results and Discussion

We applied the developed numerical scheme to perform several simulations with varying combinations of *activated* and *de-activated* advection- and diffusion-type process building blocks, e.g. transport and phase changes, such as also considered in Schürholt et al. (2020) vs transport and phase changes in the presence of settling, and their corresponding coupled scenarios. Furthermore, this scheme allowed the numerical verification of separate building blocks. While the scenarios are still idealized, they demonstrate the robustness of the Eulerian-Lagrangian scheme against selection of varying sub-sets of model components. Table 2 provides an overview on the various combinations we considered, as they have been introduced in Sect. 3. Note that we used the terms vertical velocity and settling velocity interchangeably.

Firstly, we focus on the effects due to pure mechanical settling on the snowpack (Case 1). Next, we consider isolated heat transport (Case 2) as well as its interplay with settling processes (Case 3). Similarly, we consider coupled heat and water transport first in the absence of settling (Case 4), later with settling (Case 5). For Case 5, we evaluate the effect of included or excluded

https://doi.org/10.5194/tc-2021-73
Preprint. Discussion started: 25 March 2021

The Cryosphere Discussions
Open Access
EGU

Table 2. List of the various simulation scenarios, referred to as *Cases*, in which we activate different combinations of process building blocks and consider a constant and non-constant viscosity closures. Heat transport induces vapor transport and triggers phase changes. Case 5 and Case 7 are also referred to as *fully coupled processes*.

Case	**Heat Transport** (Eq. (23))	**Vapor transport** (Eq. (24))	**Mechanics** (Eqs. (19) and (20))			
			Viscosity (Sect. 2.3)		**Glen's law** (Eq. (17))	
			$\eta = const$	$\eta(\phi_i, T)$	$m = 1$	$m = 3$
Case 1			✓		✓	
Case 2	✓					
Case 3	✓		✓		✓	
Case 4	✓	✓				
Case 5	✓	✓	✓		✓	
Case 6				✓	✓	
Case 7	✓	✓		✓	✓	
Case 8	✓	✓	✓			✓

error terms $\mathbf{E}_T$ and $\mathbf{E}_c$ (cf. Sect. 3.4) on the temperature profiles. Case 1, Case 3, and Case 5 consider the constant viscosity for linear Glen's law ($m = 1$) $\eta_{const,m=1}$, as introduced in Sect. 2.3. Furthermore, we investigate the impact of an empirical, temperature and ice volume fraction controlled, viscosity closure (Eq. (4)), first on settling only (Case 6) and then on the fully coupled processes (Case 7). Next, we show that our general approach can be combined with the non-linear Glen's law (Eq. (3)) by using $m = 3$ (Case 8) and an accordingly adjusted constant viscosity $\eta_{const,m=3}$. For a detailed explanation of the general derivation of the viscosity values see Sect. 2.3. Lastly, we compare our new modeling approach to that of a layer-based scheme (Sect. 1).

4.1 Computational setup, initial and boundary conditions

Initial condition: The initial ice volume fraction ϕ_i reflects a layered situation as depicted in Fig. 3, with two snow layers of equal thickness. The bottom layer has an initial effective density of 150 $\mathrm{kg\ m^{-3}}$, and the upper layer's density is 75 $\mathrm{kg\ m^{-3}}$. The densities are in the range of "damped new snow" and "new snow" respectively (Paterson, 1994). The transition from the upper layer to the lower layer is linearly smoothed out over over 2 cm, which for a grid defined according to Sect. 3.2 corresponds to 5 computational nodes for the coarser and 11 computational nodes for the finer discretization. Temperature is initially constant at a value of 263 K throughout the whole snowpack. Deposition rate is directly deduced from temperature (see 3. in Sect. 3.5) and therefore requires neither initial nor boundary condition. From the initial condition we derived the constant viscosity values $\eta_{const,m=1} \approx 9.1 \times 10^7$ Pa s and $\eta_{const,m=3} \approx 16 \times 10^{12}$ Pa s, see also Appendix A3.

Boundary condition: We consider a constant temperature of 273 K at the bottom boundary, and a constant temperature of 253 K at the free surface. **Simulation time:** We simulate 2 days (48 h), 3 days (62 h), and 4 days (96 h) scenarios.

https://doi.org/10.5194/tc-2021-73
Preprint. Discussion started: 25 March 2021

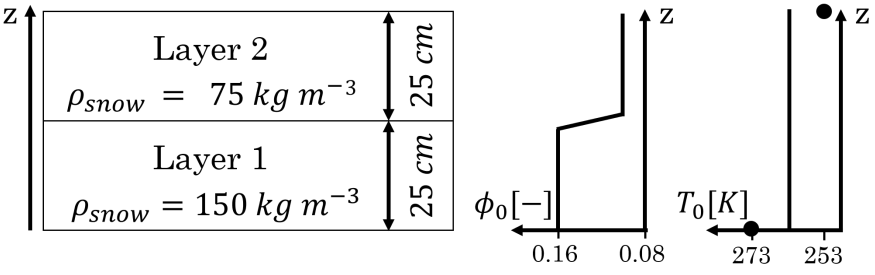

Figure 3. Shows the initial condition of the snowpack regarding snow density at the left hand side and profile plots of the initial ice volume fraction ($\phi_{i,0}$) and temperature (T_0) at the right hand side. There are two snow layers with equal thickness of 25 cm, yielding a snowpack of height 50 cm. The bottom layer has a higher density value of 150 kg m^{-3} and the upper layer's density is 75 kg m^{-3}. The z-axis of the 1d model increases in upward direction, so that $z = 0$ denotes the ground. Downward directed movements are thus described by negative velocities. The interface between the two layers is referred to as transition area. The initial ice volume fraction is derived from initial snow density. Its profile ($\phi_{i,0}$) shows the linear decrease of ice volume fraction in the transition area from the lower to the upper layer. The initial temperature profile (T_0) is constant at 263 K. The black dots mark the constant temperature boundary conditions: 273 K at the bottom; and 253 K at the top.

4.2 Settling (Case 1)

As the first step, we investigate the effects of mechanical settling on the snowpack (Case 1 in Table 2) and in particular the evolution of the vertical velocity (Fig. 4 (a)) and the ice volume fraction (Fig. 4 (b)). The vertical velocity decreases from top to bottom and relaxes during the first 48 h. Furthermore, the vertical velocity varies less in the upper layer than it does in the lower layer. This effect is due to the increase of the overburdened snow mass from top to bottom. Settling proceeds the fastest just after the start of the simulation, when the snowpack is at maximum height and correspondingly its effective density is the lowest. In the course of time the ice volume fraction increases faster in the lower layer than in the upper layer, and it is the highest at the bottom of the snowpack (Fig. 4 (b)). Furthermore, the extent of the upper layer decreases only slightly with time, whereas the lower layer reduces to half of its initial height. These effects are expected and reflect the correlation between the amount of compaction and the total overburdened mass.

4.3 Heat transport in the absence and presence of settling (Cases 2 and 3)

First, we consider isolated heat transport. This simulation scenario refers to Case 2 in Table 2. Temperature (Fig. 5 (a)), and temperature gradients (Fig. 5 (c)) reach a stationary state after approximately 60 h. Heat flux differences between the two layers are clearly visible in the temperature gradient plot. Next, heat transport is superposed by mechanical settling (Fig. 5 (b) and (d)), representing Case 3. As a result, snow height decreases while the internal temperature profiles evolve. Active mechanical processes yield a steepened temperature gradient, hence a higher value of the heat flux (Fig. 5 (d)). This effect can be attributed to:

https://doi.org/10.5194/tc-2021-73
Preprint. Discussion started: 25 March 2021

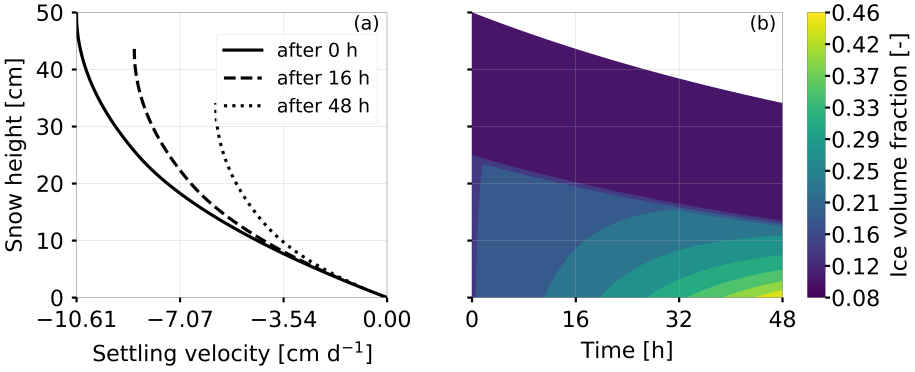

Figure 4. Plots show the results of Case 1 of Table 2, corresponding to isolated settling effects. (a) depicts vertical velocity over snow height. The profiles show the state of the snowpack at initiation, after 16 h and after 48 h. It is clearly visible that vertical velocity and the absolute snow height decrease with time. (b) depicts ice volume fraction over time. Changes of the ice volume fraction are visible in the lower layer; it increases most at the bottom of the snowpack.

- the decrease of snow height while keeping the temperatures at the boundaries fixed, and
- the permanent change of thermal conductivity and thermal diffusivity due to their dependency on variations in the ice volume (Eq. (A3)).

The temperature profile will reach the stationary state once the ice volume fraction has reached its maximum value.

4.4 Heat and vapor transport in the absence and presence of settling (Cases 4 and 5)

By using the vapor formulation from Hansen and Foslien (2015), transport of vapor through and phase changes in the snowpack both require an apparent temperature gradient, such that the solution of vapor transport should only be considered in conjunction with heat transport here (Cases 4 and 5 in Table 2). In Fig. 6 (a), we compare the deposition rate (negative for sublimation) due to heat and vapor transport only (Case 4) with the deposition rate obtained when considering additional settling processes, representing the fully coupled processes (Case 5). Both profiles are characterized by moderate deposition rates throughout the snow column with a pronounced negative (sublimation) peak at the centre of the snow column, which is located in the transition area of the layers. This is interpreted as the onset of spatio-temporal oscillations as observed and investigated in greater detail in the companion paper (Schürholt et al., 2020). It nicely demonstrates that a) our Eulerian-Lagrangian scheme can capture this behavior, and b) that the instability prevails even in the presence of settling processes. In fact, the fully coupled processes shows an even higher sublimation peak (approximately 4 times). Figure 6 (b) shows the time evolution of the fully coupled processes. In the first hours, there is low sublimation taking place in the transition area. After about 6 hours, a pronounced sublimation rate peak starts to develop that keeps increasing until 48 h. The increased sublimation may be driven by strong vapor density gradients above the transition area that can be inferred from a strong temperature gradient in that area. This temperature variation is further enhanced by compaction due to settling (Fig. 5). The results suggest that mechanics likely

https://doi.org/10.5194/tc-2021-73
Preprint. Discussion started: 25 March 2021

The Cryosphere
Discussions
Open Access
EGU

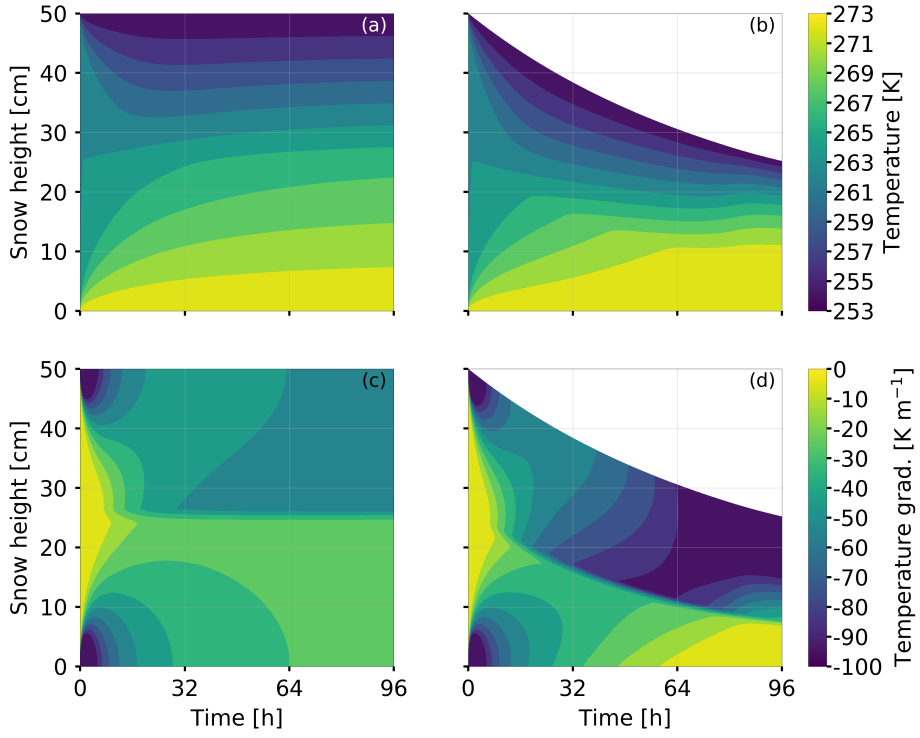

Figure 5. (a) and (c) show the results for Case 2 of Table 2 corresponding to heat transport solely active. (b) and (d) show the results for Case 3 of Table 2 corresponding to active heat transport and mechanical settling. For each plot y-axis represents snow height and x-axis time. The plots in the top row ((a) and (b)) show the temperature evolution, and the plots in the bottom row ((c) and (d)) show the respective temperature gradients. The initial condition for both cases are equivalent (see Fig. 3). In Case 2 the temperature profile (a) has reached the stationary, piecewise linear profile after approximately 60 h. In Case 3 the temperature profile (b) is not yet stationary at the end of the simulation (96 h) as mechanical processes are still yielding a change in ice volume fraction. The temperature gradient (c) will become constant, only when the maximum ice volume fraction has been reached.

increase local phase change activity in the vicinity of layer boundaries, which potentially has a large effect on weak layer formation. Lastly, we evaluated the effect of the error terms as introduced in Sect. 3.4 for Case 5. To do so, we derived the weighted mean of the deviations of the temperature distribution obtained without error terms from that with error terms in Eqs. (23) and (24). The error increases with simulation time and is 0.017 after 24 h, 0.063 after 36 h, and 0.183 after 48 h. After 48 h the deviation is highest for the computational nodes just above the layer transition, where high temperature gradients are present (cf. Fig. 5).

4.5 Settling-induced evolution of the ice volume fraction in the absence and presence of transport (Cases 1 and 5)

In this section, we compare isolated settling (Case 1 in Table 2) and the fully coupled processes (Case 5 in Table 2) with respect to their impact on the evolving ice volume fraction. Figure 7 shows the corresponding ice volume fraction profiles after 2 days.

https://doi.org/10.5194/tc-2021-73
Preprint. Discussion started: 25 March 2021

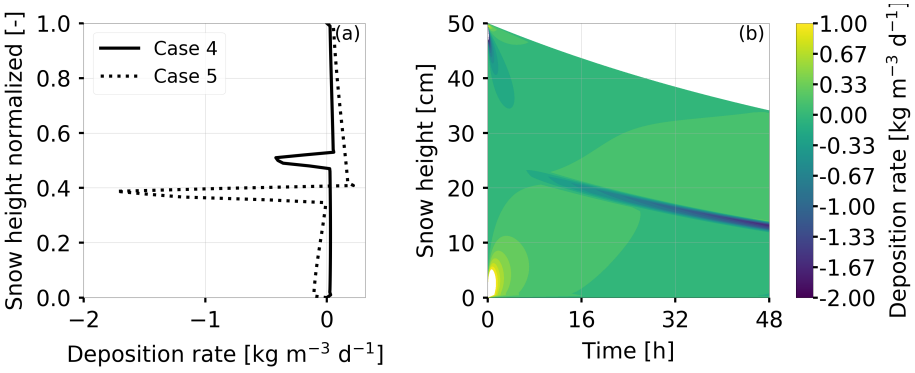

Figure 6. (a) shows two deposition rate profiles over normalized snow height after 2 days. The solid line represents the results of heat and vapor transport in the absence of settling for Case 4 of Table 2. The dashed line refers to Case 5 of Table 2 that additionally accounts for settling. Sublimation rates (negative deposition rates) for Case 5 (fully coupled processes) are increased by approximately a factor of 4 with respect to a Case 4 without settling. (b) shows the deposition rate profile evolution for Case 5. A pronounced sublimation rate peak in the transition area is first visible after approximately 6 h and increases with time. The lobes at the top and bottom at the start of the simulation are due to the strong phase change activity triggered by the initial and boundary conditions.

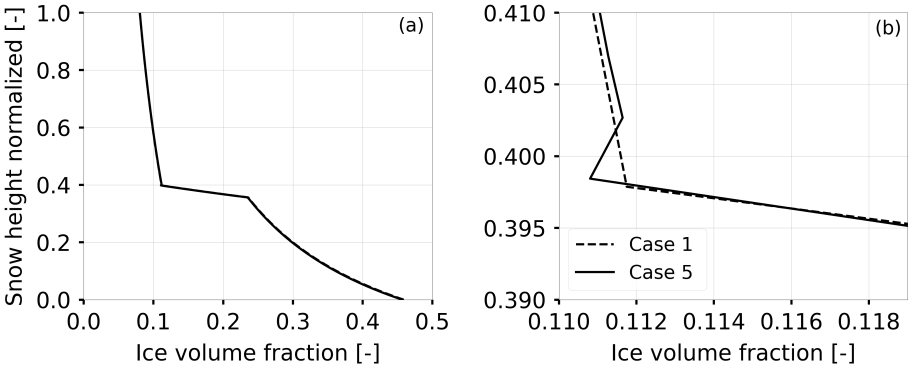

Figure 7. The plots show ice volume fraction profiles over normalized snow height after 2 days. The dashed line (a) depicts ice volume fraction for Case 1 of Table 2 corresponding to solely active settling, whereas the solid line depicts ice volume fraction computed based on Case 5, which refers to the fully coupled processes. (b) zooms into the density transition area of (a) and shows the effect of the increased sublimation in Fig. 6 on ice volume. In order to better resolve the kink of Case 5, we increased the number of grid nodes to 251.

Both profiles are very similar, which suggests that the density evolution is dominated by settling processes, whereas coupled heat and vapor transport play a minor role. When focusing on the upper boundary of the transition area (Fig. 7 (b)), we however find a localized decreased ice volume fraction for the fully coupled processes (Case 5). This suggests a localized ice volume decay for active vapor transport and implies phase changes. This observation is consistent with the earlier observed enhanced sublimation rate in Fig. 6 indicating the formation of a density heterogeneity.

https://doi.org/10.5194/tc-2021-73
Preprint. Discussion started: 25 March 2021

The Cryosphere Discussions
Open Access
EGU

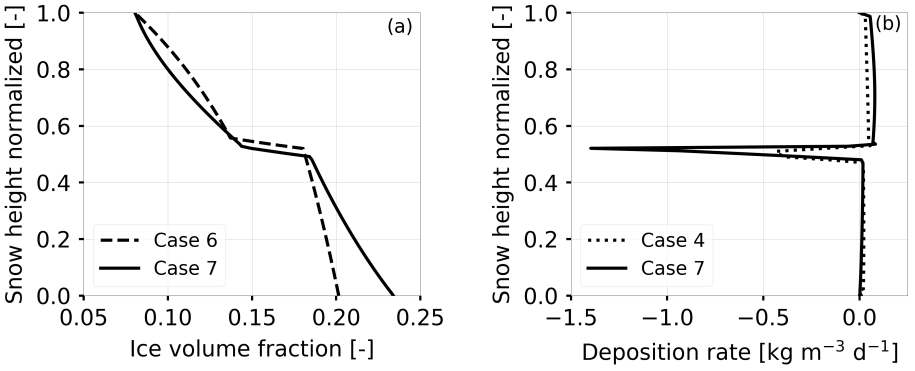

Figure 8. (a) shows ice volume fraction profiles after 3 days simulation time obtained with a dynamic viscosity. Y-axis depicts normalized snow height. The dashed line refers to Case 6 of Table 2 corresponding to mechanical settling solely, and the solid line refers to Case 7, which represents the fully coupled processes. (b) shows deposition rate profiles for Case 7 and Case 4 after 3 days simulation time. Y-axis depicts normalized snow height. The solid line refer to Case 7, and the dashed line represents heat and vapor transport in the absence of settling (Case 4). For the fully coupled processes sublimation rate at the layer transition is approximately three times stronger compared with inactive settling (Case 4).

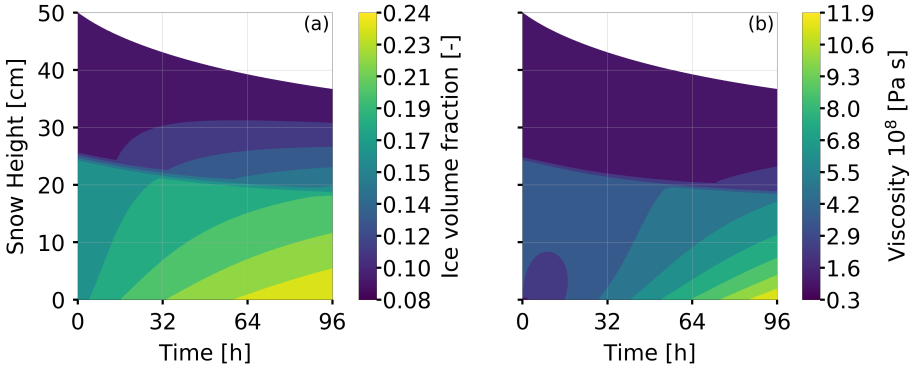

Figure 9. The plots show the evolution of ice volume fraction (a) and viscosity (b) for 4 days for Case 7 of Table 2, which refers to the fully coupled processes combined with dynamically varying viscosity. Snow height is depicted on the y-axis. In (a) ice volume fraction increases most at the bottom of the upper layer. The lower layer consolidates less than the upper layer. In (b) viscosity increases slower in the upper layer and increases faster (up to one magnitude) in the lower layer.

Figure 9, finally, shows the evolution of ice volume fraction and viscosity over time for 4 days. Ice volume fraction increases gradually throughout the snow column (Fig. 9 (a)). In Fig. 9 (b), we see that the viscosity of the upper layer has smaller values and also increases slower compared to viscosity values in the lower layer. In contrast, viscosity increases by approximately one magnitude in the lower layer. The height of the lower layer decreases less than the height of the upper layer. This outcome may be related to the lower layer's higher viscosity (higher resistance to deformation).

https://doi.org/10.5194/tc-2021-73
Preprint. Discussion started: 25 March 2021

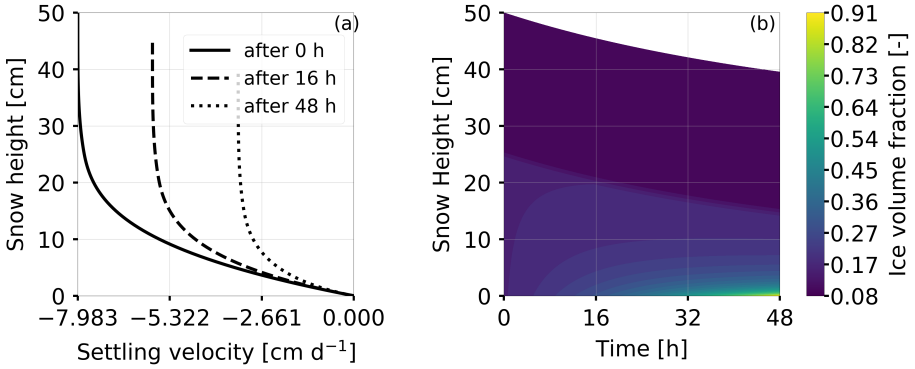

Figure 10. The plots show vertical velocity profiles (a) and ice volume fraction (b) for Case 8 of Table 2, which refers to the fully coupled processes combined with a non-linear Glen's law. Velocity (a) varies less, which yields a more uniform evolution of the snowpack (b).

4.6 Linear versus non-linear Glen's law in a fully coupled dry snowpack model of constant viscosity (Cases 5 and 8)

In the final simulation scenario, we compare results of the fully coupled processes for different parameters in Glen's law (Eq. 3), namely $m = 1$ in Case 5 and $m = 3$ in Case 8). As discussed before, the viscosity closure (whether it is a constant value or an empirical closure) strongly depends on the choice of the Glen parameter m. This requires us to adjust the constant viscosity value accordingly, see Sect. 2.3 for details.

Figure 10 (a) shows vertical velocity profiles and the evolution of ice volume fraction with time. The vertical velocity is almost constant in the upper layer and then decreases in the lower layer. This effect is similar to the vertical velocity profiles as presented and explained in Sect. 4.2, but it is more pronounced due to the non-linearity in the constitutive law. Compared with previous scenarios, the overall vertical velocity is lower. This is probably related to the magnitude of the constant viscosity and cannot be directly related to the non-linear constitutive law. A further sensitivity study in the future would be most informative. In Fig. 10 (b) the upper layer's ice volume fraction and thickness remains almost constant with time. In contrast, the lower layer decreases in height, while the ice volume fraction increases with time from top to bottom.

Again, the corresponding deposition rate profile shows a sublimation peak in the layer transition area (Appendix D1) that increases with time. Overall however, deposition rates tend to be lower compared to preceding computations. The reduced phase change activity in the layer transition area can directly be related to smaller vertical variations in the temperature profile. This effect may be due to less variation in the vertical velocities that yield a more uniform deformation and a less pronounced variation of ice volume fraction across the layer transition area.

4.7 Comparison against layer-based schemes (based on Case 6)

In this section, we compare results of our proposed Eulerian-Lagrangian scheme with conventional layer-based models. We would like to emphasize that a two layer snowpack model certainly constitutes an extremely simplified case, as layer-based schemes are usually operated with a significantly higher number of snow layers. It is yet informative to conduct this analysis

https://doi.org/10.5194/tc-2021-73
Preprint. Discussion started: 25 March 2021

to point out this differences, as these can certainly accumulate during long simulation times.

In layer-based snowpack models state variables are assigned layerwise, and the two layer snowpack (Fig. 3) would have three computational nodes at the following locations: at the bottom of Layer 1, at the top of Layer 1 and at the top of Layer 2. The two nodes located at the top of the layers would then represent the physical state of Layer 1 and Layer 2, respectively. Velocity is again derived from stress exerted by the overburden snow mass. Since Layer 2 is represented by the computational node at the top, it is unloaded and requires a special treatment for stress. We adopt the approach by Vionnet et al. (2012) and apply a 'non-physical stress' equivalent to half of the layer's own weight, yet apply it to the uppermost computational node (Sect. 3.4 in Vionnet et al. (2012)). Next, vertical velocity is computed likewise with Eq. (7) and viscosity with Eq. (4). We compare both approaches based on Case 6 of Table 2, hence in the presence of mechanical settling and for a dynamic viscosity closure. Since we neglect heat and vapor transport, the viscosity changes over time are solely due to the evolution of ice volume fraction alone.

In Fig. 11, we see that the layer-based scheme sustains a layer-based vertical velocity (a) and ice volume fraction evolution (c): One value for the velocity and one value for the ice volume fraction describe an entire layer. In contrast, using the generalized Lagrangian approach described in Sect. 3, we yield a sublayer resolution of the vertical velocities (b) and ice volume fractions (d). For both approaches (layer-based and Eulerian-Lagrangian) the vertical velocity is higher in the top part of the snowpack and zero at the bottom. For early times, the layer-based scheme determines a vertical velocity that is one order of magnitude higher than values computed with the Eulerian-Lagrangian scheme. This may be related to the comparably high (non-physical) stress at the top of Layer 2. At the end of the simulation, the snowpack has settled almost twice as much with the layer-based scheme, which highlights the impact of this conceptual difference. This effect may result from an overestimation of velocity with layer-based schemes. Following our proposed method, ice volume fraction is higher in the lower part of the snowpack and reaches higher values (Fig. 11 (d)). Furthermore, ice volume fraction at the top of the snowpack does not change during the simulation since there is no stress from overburden mass. In contrast, for the layer-based scheme ice volume fraction grows at this location (Fig. 11 (c)). This is again due to the chosen stress condition at the top. Of course this discrepancy gets smaller as we increase the number of layers and this effect may reduce. However this slight offset in the stress condition will always be present and lead to uncertainties. In the proposed computational approach the spatial resolution of processes can be easily changed to assess its impact on snowpack evolution. In a future study, it might be interesting to quantitatively compare results against Jafari et al. (2020), who also rely on a rather fine spatial resolution.

5 Summary and conclusions

In this article, we described in detail a hybrid Eulerian-Lagrangian computational approach to model the evolution of a dry snowpack. The model accounts for transport of heat and vapor, phase changes (sublimation and deposition), and mechanical settling processes. The ice mass balance is explicitly accounted for in the model formulation. It captures the evolution of the ice volume fraction in response to settling and phase changes. It constitutes an advection-dominated partial differential equation of hyperbolic type, and is therefore conveniently solved with the method of characteristics, a popular Lagrangian type

https://doi.org/10.5194/tc-2021-73
Preprint. Discussion started: 25 March 2021

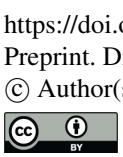

The Cryosphere Discussions
Open Access
EGU

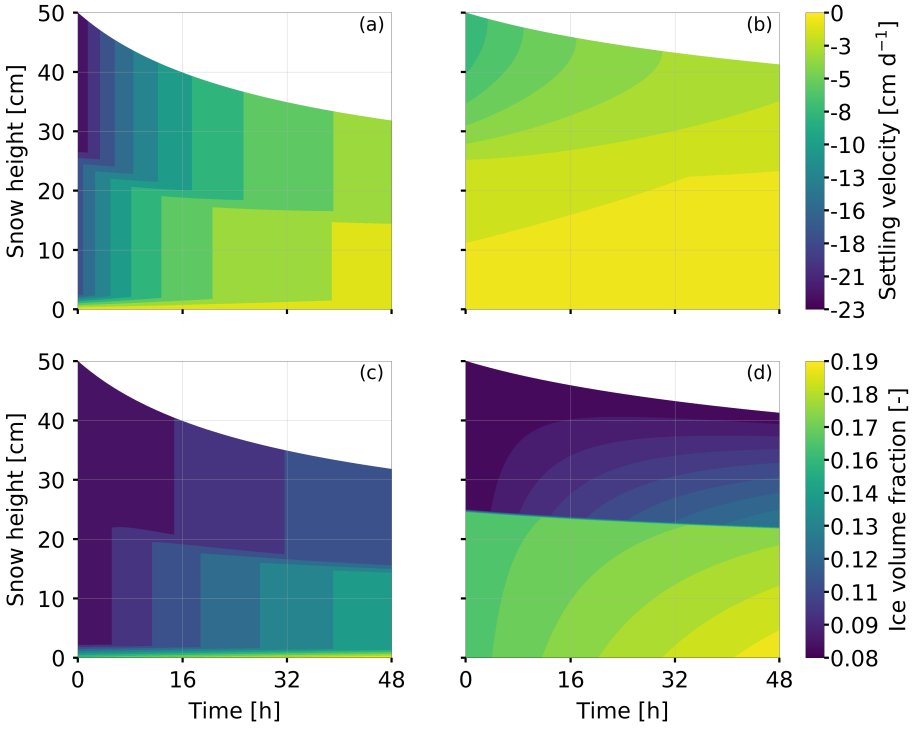

Figure 11. The plots show the temporal evolution of vertical velocity (top row) and ice volume fraction (bottom row) for Case 6 of Table 2 corresponding to solely active mechanical settling. For (b) and (d), we applied our highly discretized settling scheme, and for (a) and (c), we mimicked the layer-wise discretization of layer-based schemes. Y-axis depicts snow height. Snow viscosity is controlled by ice volume fraction alone, since heat transport is inactive. In (a) and (c) Layer 1 and Layer 2 are resolved. Their respective values refer to the computational nodes at the top and between the two layers. The values retrieved for the lowest node, do not represent an entire layer and are depicted at height zero. For the layer-based scheme, one velocity or ice volume fraction value represents the movement or density of the entire layer. In contrast, with our approach vertical velocity varies throughout each layer (b) so that ice volume fraction increases layer internally and develops a gradual pattern (d).

scheme for such processes. Here, Lagrangian refers to the fact that the scheme tracks the motion of a snow material "particles" within the snow column by adjusting the node positions, while at the same time it accounts for phase changes within the moving particle. Solving the ice mass balance requires us to specify the vertical velocity as well as the mass production rate (sublimation rate/deposition rate). A closure for the velocity is derived by combining a common mechanical stress-strain
505 relation with Glen's law, and numerically approximating the resulting integrals. The deposition rate is due to vapor transport through a varying temperature field, and can be determined from a diffusive type process model that accounts for simultaneous heat and vapor transport. Due to its diffusive type (parabolic), a fixed-grid approach is most appropriate, referred to as an Eulerian approach. More specifically, we solved coupled heat and vapor transport by means of a first order implicit in time finite difference approximation. The Eulerian scheme for the process model's diffusive part complies with the non-uniform

https://doi.org/10.5194/tc-2021-73
Preprint. Discussion started: 25 March 2021

mesh that results from the Lagrangian scheme for the ice volume fraction evolution. In order to solve the complete dry snow process model for the coupled evolution of the ice volume fraction, temperature field, vapor field and settling processes, the Eulerian and Lagrangian parts are iteratively applied following a straight-forward operator split approach.

We have implemented our proposed numerical scheme as a series of sequential updates within one simulation time step. The implementation follows a modular, extendable approach, such that each process building block can easily be considered or neglected for verification or validation purposes. We applied our numerical core to conduct a series of simulation scenarios comprising isolated processes (pure settling, pure heat transport), two-process coupling scenarios (heat transport in the presence of settling, coupled heat and vapor transport) and the fully coupled processes (heat and vapor transport in the presence of settling). We furthermore investigated different viscosity closures as well as a linear and a non-linear version of Glen's law. A two-layer snowpack, consisting of a lower layer of higher density and an upper layer of lower density, served as a test case to demonstrate the feasibility of our approach. We simulated fields and profiles for temperature, deposition rate, ice volume fraction and vertical velocity with a high spatial (~mm to cm) and temporal (~min) resolution.

We found that

- Our Eulerian-Lagrangian scheme along with its vectorized implementation is flexible and extendable. Alternative model closures, e.g. for the viscosity and the vertical velocity can easily be integrated. To close for the velocity, we have successfully tested a non-linear strain rate closure commonly used in firn models (Lundin et al., 2017). The Lagrangian part of the solver (that accounts for the evolution of the ice volume fraction) could easily be singled out and coupled to an alternative process model, e.g. when accounting for firn conditions instead of dry snow.

- Although within this paper, we mostly relied on numerical approximations that are of either first order (time integration/operator splitting) or second order (diffusion operator), the corresponding numerical solvers can be extended without a conceptual difficulty, e.g. changing from a first order time integration to an higher order in time integrator. We commented on this in the respective section.

- The combination of an implicit Eulerian routine for the diffusion-dominated operators (that controls the time stepping) and a Lagrangian routine for the advection-dominated operators ran stable and robust for all considered simulation cases (different viscosity closures, different versions of Glen's law).

- The numerical scheme allows for a high spatial resolution that resolves processes on the sublayer level. By construction, it relies on a mechanically consistent vertical velocity. This improves the accuracy since it makes the ad-hoc specification of an artificial stress value for the uppermost layer Vionnet et al. (2012), as required for conventional layer-based schemes, obsolete.

- The modular setup of the software facilitated a systematic study of various models formulations, in which we selectively considered different combinations of process building blocks without fine-tuning the stability of the solver. This is important to enable empirical-numerical investigations of the relevance of different process couplings (see next point).

https://doi.org/10.5194/tc-2021-73
Preprint. Discussion started: 25 March 2021

– Our simulation consistently showed that vapor transport and phase change in the presence of strong temperature gradients can induce a stronger phase change activity, and in particular a localized sublimation rate peak above the transition area between two layers. We furthermore showed that this has the potential to result into a localized ice volume fraction reduction above the transition area. This in itself is not new, as a similar behavior has been deduced in Hansen and Foslien (2015) and analyzed in detail in our companion paper Schürholt et al. (2020). In addition to the existing results, however, we have shown that the increased phase change activity persists in the presence of settling (even more pronounced), for both a constant and a dynamic viscosity closure, and for a linear as well as a non-linear version of Glen's law.

– The incorporation of the Error terms in the vapor and heat transport equations that account for deviations due to the non-uniform mesh increases accuracy especially in areas with large node distances and high temperature gradients.

In our article, we deliberately focused on discussing modularity and extendability in the context of snowpack modeling, e.g. by assessing a whole process cascade for one relatively simplified physical setting. In order to discuss these aspects in-depth, we restricted ourselves to one relatively simply physical setting. We are well aware that as of today, our proposed numerical approach is not ready for operational use, and that was not our intention. At this point in time, we rather would like to contribute to the discussion how future snowpack modeling can benefit from a consistently formulated, hybrid Eulerian Lagrangian solver. Nevertheless, it is important to discuss, whether the suggested scheme is amenable to further extensions required for an operational snowpack model.

Most importantly, the proposed scheme would need a generalization for surface mass gain (precipitation) or losses (sublimation). This bears two technical challenges. First, concurrent settling and precipitation result in a non-monotonic vertical motion of the snowpack's upper surface, for which several techniques have been proposed in the past, e.g. based on a regularization approach (Wingham, 2000) or via a kinetic boundary conditions as applied for sedimentation on ocean floors in (Audet and Fowler, 1992). A straight-forward approach based on appending the computational grid sequentially during precipitation events likewise seems computationally feasible. A second challenge associated with the incorporation of precipitation events is the question of how to initialize the complete state (temperature, vapor and deposition rate) in the new snow layers. The latter is less critical in conventional layer-based schemes, as the necessary information reduces to 'one value per layer'. While the first challenge mostly means to overcome technical subtleties in the actual implementation, the second requires a thoughtful formulation of physically consistent boundary conditions. Neither of the two challenges seem to pose a severe risk.

Another important addition to our proposed snowpack model is the presence of liquid water in the snow. While its pure including potential phase changes could be straight-forwardly implemented, it is the advective transport of liquid water that is more demanding. Liquid water transport is commonly modeled via the Richards equation (Wever et al., 2014) which would benefit from existing hybrid Eulerian-Lagrangian solution strategies, as shown for saturated media without mechanical settling (Huang et al., 1994). Once set up, it can be integrated into our computational workflow (Fig. 2).

Finally, operational models generally include the capability to account for topological change within the snow column, to capture layer coalescence if two initially separated snow layers merge into one, or layer separation, if an initially homogeneous layer splits into two. By construction, our computational approach does not require a dedicated treatment for layer coalescence

https://doi.org/10.5194/tc-2021-73
Preprint. Discussion started: 25 March 2021

or separation. Both are implicitly accounted in the continuous description of stratigraphy as long as the feature that is to be resolved is larger than the chosen spatial resolution of the computational grid. Otherwise the resolution can be increased to avoid layer split ups for regions with high gradients. Furthermore, our approach prevents the complete degeneration of layers as the ice volume fraction is constrained by the snow's maximum apparent density per construction of the scheme. Yet, while the theory suggests that layer coalescence and separation are not problematic, their might still be troublesome realistic test cases, especially when thinking about long simulation times. In order to address these and verify robustness, a series of benchmark tests have to be conducted. If necessary, the Lagrangian-Eulerian scheme in its current version can be equipped with occasional re-meshing (along with a re-sampling of field variables) triggered by the degeneration of well defined mesh quality criteria.

We believe that a flexible and extendable computational approach, such as the one described in this article, will be key for future snowpack modeling, to facilitate the use of standardized benchmark problems (potentially used during a continuous integration) and allow us to systematically assess the model's predictive power, including uncertainty quantification, parameter estimation and model selection.

https://doi.org/10.5194/tc-2021-73
Preprint. Discussion started: 25 March 2021

Code availability. The code will be made available upon acceptance.

Appendix A: Formulas required for the process model

A1 Vapor saturation density

An empirical expression for the vapor saturation density $\rho_v^{eq}(T)$ in terms of temperature T is formulated based on the empirical formulation for vapor saturation pressure from Libbrecht (1999) and reads

$$\rho_v^{eq}(T) = \frac{exp(-\frac{T_{ref}}{T})}{fT}(a_0 + a_1(T-273) + a_2(T-273)^2) \tag{A1}$$

with coefficients $a_0 = 3.6636 \times 10^{12}$, $a_1 = -1.3086 \times 10^8$, $a_2 = -3.3793 \times 10^6$, $f = 461.31$ as well as reference temperature $T_{ref} = 6150$ K. Note that fT accounts for the conversion from Pa to kgm^{-3} with the ideal gas law.

A2 Model parameters in the transport and phase change equations

The effective vapor mass diffusion coefficient $D_{eff}(\phi_i)$ in terms of ice volume fraction ϕ_i is taken from Calonne et al. (2011), but is extended by the heaviside function HS to hinder vapor diffusion for ice volumes above $\frac{2}{3}$

$$D_{eff}(\phi_i) = D_0(1 - \frac{3}{2}\phi_i)\, HS\left(\frac{2}{3} - \phi_i\right), \tag{A2}$$

with $D_0 = 2.036 \times 10^{-5}\ \mathrm{m^2 s^{-1}}$ the vapor diffusion constant in air.
The effective thermal conductivity $k_{eff}(\phi_i)$ in terms of ice volume fraction ϕ_i is taken from Calonne et al. (2011) and reads

$$k_{eff}(\phi_i) = a_0 + a_1(\phi_i\, \rho_i) + a_2(\rho_i\, \phi_i)^2 \tag{A3}$$

with coefficients $a_0 = 0.024$, $a_1 = -1.23 \times 10^{-4}$ and $a_2 = 2.5 \times 10^{-6}$ and ice density ρ_i.
The effective heat capacity $(\rho C)_{eff}(\phi_i)$ in terms of ice volume fraction ϕ_i is taken from Calonne et al. (2014) and Hansen and Foslien (2015) and reads

$$(\rho C)_{eff}(\phi_i) = \phi_i\, \rho_i\, C_i + (1 - \phi_i)\, \rho_a\, C_a, \tag{A4}$$

with C_i ice heat capacity, C_a air heat capacity and ρ_i ice density.

A3 Constant viscosity for the two layer case

A3.1 Linear Glen's law, $\eta_{const,m=1}$

We derived intermediate ice volume fraction $\phi_{i,const} = 0.1125$ and temperature $T_{const} = 263$ K values from the initial condition of the two layer case and insert them as constants into Eq. (4).

https://doi.org/10.5194/tc-2021-73
Preprint. Discussion started: 25 March 2021


The Cryosphere Discussions
Open Access
EGU

A3.2 Non-linear Glen's law $\eta_{const,m=3}$

Equation (4) does not hold for Glen exponent $m = 3$, therefore we derive an adjusted constant viscosity $\eta_{const,m=3}$ via the constitutive equation (Eq. (3))

$$\dot{\epsilon}_{lit} = \frac{1}{\eta_{const,m=3}} \sigma_{max}^{m}, \tag{A5}$$

with $\dot{\epsilon}_{lit} \equiv 10^{-6}$ s^{-1} a strain rate value from the literature Johnson (2011) and $\sigma_{max} \equiv 547.71$ Pa the maximum stress value obtained from the initial snow density profile of the two layer case. Eq. (A5) is then solved for the constant viscosity $\eta_{const,m=3}$.

A3.3 Restrict infinite ice volume growth

To hinder infinite ice volume growth, the constant viscosity $\eta_{const,m}$ is combined with a power law that yields exponential growth of viscosity for cells with $\phi_i > 0.95$

$$PL(\phi_i) = exp\,(pl1\,\phi_i - pl2) + 1, \tag{A6}$$

with $plt1 = 690$ and $pl2 = 650$. The constant viscosity is then multiplied with the power law ($\eta_{const,m}\,PL(\phi_i)$), so that computational nodes with $\phi_i > 0.95$ are assigned and viscosity grows exponentially. Note that for better readability the multiplication with the power law is omitted in the equations of this paper.

Appendix B: Mesh error terms due to non-uniform mesh

For the temperature equation Eq. (23) the mesh error term is

$$E_T(T_{k+1}^n, T_k^n, T_{k-1}^n) = \frac{\Delta z_k^n - \Delta z_{k-1}^n}{\Delta z_k^n + \Delta z_{k-1}^n} \frac{2 \cdot \left(\beta_T \left(T_{k+1}^{n+1} - T_k^{n+1}\right) - \beta_T \left(T_k^{n+1} - T_{k-1}^{n+1}\right)\right)}{\left(\Delta z_k^n\right)^2 + \left(\Delta z_{k-1}\right)^2}, \tag{B1}$$

and for the vapor transport equation Eq. (24) it is

$$E_c(T_{k+1}^n, T_k^n, T_{k-1}^n) = \frac{\Delta z_k^n - \Delta z_{k-1}^n}{\Delta z_k^n + \Delta z_{k-1}^n} \frac{2 \cdot \left(\beta_c \left(T_{k+1}^{n+1} - T_k^{n+1}\right) - \beta_c \left(T_k^{n+1} - T_{k-1}^{n+1}\right)\right)}{\left(\Delta z_k^n\right)^2 + \left(\Delta z_{k-1}\right)^2}. \tag{B2}$$

For the matrix equations Eqs. (26) and (25) the mesh error terms are defined as $\mathbf{E}_T$ and $\mathbf{E}_C$.

https://doi.org/10.5194/tc-2021-73
Preprint. Discussion started: 25 March 2021

The Cryosphere Discussions
Open Access
EGU

Appendix C: Matrices from temperature and vapor transport equations

Matrix $\mathbf{A}$ is defined as follows:

$$\mathbf{A} = \begin{pmatrix} A^n_{m,0} & 0 & 0 & \cdots & 0 & 0 & 0 \\ A^n_{l,1} & A^n_{m,1} & A^n_{u,1} & \cdots & 0 & 0 & 0 \\ 0 & A^n_{l,2} & A^n_{m,2} & \cdots & 0 & 0 & 0 \\ \vdots & \vdots & \vdots & \ddots & \vdots & \vdots & \vdots \\ 0 & 0 & 0 & \cdots & A^n_{m,nz-2} & A^n_{u,nz-2} & 0 \\ 0 & 0 & 0 & \cdots & A^n_{l,nz-1} & A^n_{m,nz-1} & A^n_{u,nz-1} \\ 0 & 0 & 0 & \cdots & 0 & 0 & A^n_{m,nz} \end{pmatrix} \tag{C1}$$

For the heat equation (Eq. (25)) ($\mathbf{A}_T$) the entries are

$$A^n_{l,k} = -D^n_k \left(\beta^n_{T,k} + \beta^n_{T,k-1}\right) \tag{C2}$$

$$A^n_{u,k} = -D^n_k \left(\beta^n_{T,k+1} + \beta^n_{T,k}\right) \tag{C3}$$

$$A^n_{m,k} = \alpha^n_{T,k} + D^n_k \left(\beta^n_{T,k+1} + 2\,\beta^n_{T,k} + \beta^n_{T,k-1}\right) \text{ with } A^n_{m,0} = 1 \text{ and } A^n_{m,nz} = 1 \tag{C4}$$

with

$$D^n_k = \frac{\Delta t^n}{(\Delta z^n_k)^2 + (\Delta z^n_{k-1})^2}. \tag{C5}$$

For the vapor transport (Eq. (26)) ($\mathbf{A}_c$) the entries are

$$A^n_{l,k} = \frac{1}{\left(\Delta z^n_k\right)^2 + \left(\Delta z^n_{k-1}\right)^2} \left(\beta^n_{c,k} + \beta^n_{c,k-1}\right) \tag{C6}$$

$$A^n_{u,k} = \frac{1}{\left(\Delta z^n_k\right)^2 + \left(\Delta z^n_{k-1}\right)^2} \left(\beta^n_{c,k} + \beta^n_{c,k+1}\right) \tag{C7}$$

$$A^n_{m,k} = \alpha^n_{,k} + \frac{1}{\left(\Delta z^n_k\right)^2 + \left(\Delta z^n_{k-1}\right)^2} \left(\beta^n_{c,k-1} + 2\,\beta^n_{c,k} + \beta^n_{c,k+1}\right) \text{ with } A^n_{m,0} = -\alpha^n_{c,0} \text{ and } A^n_{m,nz} = -\alpha^n_{c,nz}. \tag{C8}$$

Matrix $\mathbf{B}$ is defined as follows:

$$\mathbf{B} = \begin{pmatrix} \alpha^n_{m,0} & 0 & 0 & \cdots & 0 & 0 & 0 \\ 0 & \alpha^n_{m,1} & 0 & \cdots & 0 & 0 & 0 \\ 0 & 0 & \alpha^n_{m,2} & \cdots & 0 & 0 & 0 \\ \vdots & \vdots & \vdots & \ddots & \vdots & \vdots & \vdots \\ 0 & 0 & 0 & \cdots & \alpha^n_{m,nz-2} & 0 & 0 \\ 0 & 0 & 0 & \cdots & 0 & \alpha^n_{m,nz-1} & 0 \\ 0 & 0 & 0 & \cdots & 0 & 0 & \alpha^n_{m,nz} \end{pmatrix} \tag{C9}$$

https://doi.org/10.5194/tc-2021-73
Preprint. Discussion started: 25 March 2021


The Cryosphere Discussions
Open Access
EGU

For Eq. (25) ($\mathbf{B}_T$) the entries are

$$\alpha^n_{m,k} = \alpha^n_{T,k} \tag{C10}$$

and for Eq. (26) ($\mathbf{B}_c$)

$$\alpha^n_{m,k} = \alpha^n_{c,k}. \tag{C11}$$

Matrix $\mathbf{E}$ is defined as follows

$$\mathbf{E} = \begin{pmatrix} 0 & 0 & 0 & \cdots & 0 & 0 & 0 \\ E^n_{l,0} & E^n_{m,1} & E^n_{u,1} & \cdots & 0 & 0 & 0 \\ 0 & E^n_{l,1} & E^n_{m,2} & \cdots & 0 & 0 & 0 \\ \vdots & \vdots & \vdots & \ddots & \vdots & \vdots & \vdots \\ 0 & 0 & 0 & \cdots & E^n_{m,nz-2} & E^n_{u,nz-2} & 0 \\ 0 & 0 & 0 & \cdots & E^n_{l,nz-1} & E^n_{m,nz-1} & E^n_{u,nz-1} \\ 0 & 0 & 0 & \cdots & 0 & 0 & 0 \end{pmatrix}, \tag{C12}$$

consisting of the following terms

$$E^n_{m,k} = f^n_{\Delta z,k}\,\beta^n_{r,k} - f^n_{\Delta z,k}\,\beta^n_{l,k} \tag{C13}$$

$$E^n_{l,k} = -f^n_{\Delta z,k}\,\beta^n_{r,k} \tag{C14}$$

$$E^n_{u,k} = f^n_{\Delta z,k}\,\beta^n_{l,k}, \tag{C15}$$

with

$$\beta^n_{l,k} = 0.5\left(\beta^n_{k+1} + \beta^n_k\right) \tag{C16}$$

$$\beta^n_{r,k} = 0.5\left(\beta^n_k + \beta^n_{k-1}\right) \tag{C17}$$

$$f^n_{\Delta z,k} = \frac{\Delta z^n_k - \Delta z^n_{k-1}}{\Delta z_k + \Delta z^n_{k-1}} \frac{1}{\left(\Delta z^n_k\right)^2 + \left(\Delta z^n_{k-1}\right)^2}. \tag{C18}$$

Note that $\beta = \beta_c$ for Eq. (26) and $\beta = \beta_T$ for Eq. (25), as explained in Sect. 3.4

https://doi.org/10.5194/tc-2021-73
Preprint. Discussion started: 25 March 2021

Appendix D: Additional figures

D1 Non-linear Glen's law

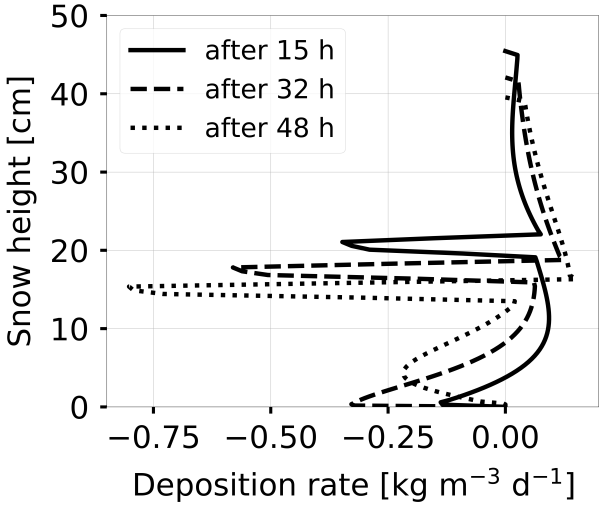

Figure D1. The plot shows the deposition rate profiles for 0, 1.5 and 2 days simulation time for Case 8 (Table 2), which is the fully coupled processes combined with the non-linear Glen's law. Y-axis depicts snow height.

Author contributions. Study concept, underlying model and methodology devised by AS, HL, and JK. Model analysis, software implementation, simulation runs performed by AS supervised by JK. Test case analysis and discussion, data visualization and manuscript preparation was carried out by AS with contributions from JK and HL.

Competing interests. No competing interests are present.

Acknowledgements. The authors were supported by the Helmholtz Graduate School for Data Science in Life, Earth and Energy (HDS-LEE). The work was furthermore supported by the Federal Ministry of Economic Affairs and Energy, on the basis of a decision by the German Bundestag (50 NA 1908).

https://doi.org/10.5194/tc-2021-73
Preprint. Discussion started: 25 March 2021

References

Audet, D. and Fowler, A.: A mathematical model for compaction in sedimentary basins, Geophysical Journal International, 110, 577–590, https://doi.org/10.1111/j.1365-246x.1992.tb02093.x, 1992.

Bader, H.-P. and Weilenmann, P.: Modeling temperature distribution, energy and mass flow in a (phase-changing) snowpack. I. Model and case studies, Cold Regions Science and Technology, 20, 157–181, https://doi.org/10.1016/0165-232x(92)90015-m, 1992.

Bartelt, P. and Lehning, M.: A physical SNOWPACK model for the Swiss avalanche warning: Part I: numerical model, Cold Regions Science and Technology, 35, 123–145, https://doi.org/10.1016/s0165-232x(02)00074-5, 2002.

Brun, E., Martin, E., Simon, V., Gendre, C., and Coleou, C.: An Energy and Mass Model of Snow Cover Suitable for Operational Avalanche Forecasting, Journal of Glaciology, 35, 333–342, https://doi.org/10.3189/s0022143000009254, 1989.

Brun, E., David, P., Sudul, M., and Brunot, G.: A numerical model to simulate snow-cover stratigraphy for operational avalanche forecasting, Journal of Glaciology, 38, 13–22, https://doi.org/10.1017/s0022143000009552, 1992.

Calonne, N., Flin, F., Morin, S., Lesaffre, B., du Roscoat, S. R., and Geindreau, C.: Numerical and experimental investigations of the effective thermal conductivity of snow, Geophysical Research Letters, 38, L23 501, https://doi.org/10.1029/2011GL049234, 2011.

Calonne, N., Geindreau, C., and Flin, F.: Macroscopic Modeling for Heat and Water Vapor Transfer in Dry Snow by Homogenization, The Journal of Physical Chemistry B, 118, 13 393–13 403, https://doi.org/10.1021/jp5052535, 2014.

Domine, F., Barrere, M., and Sarrazin, D.: Seasonal evolution of the effective thermal conductivity of the snow and the soil in high Arctic herb tundra at Bylot Island, Canada, The Cryosphere, 10, 2573–2588, https://doi.org/10.5194/tc-10-2573-2016, 2016.

Domine, F., Picard, G., Morin, S., Barrere, M., Madore, J.-B., and Langlois, A.: Major Issues in Simulating Some Arctic Snowpack Properties Using Current Detailed Snow Physics Models: Consequences for the Thermal Regime and Water Budget of Permafrost, Journal of Advances in Modeling Earth Systems, 11, 34–44, https://doi.org/10.1029/2018ms001445, 2019.

Farlow, S. J.: Partial Differential Equations for Scientists and Engineers, Dover Publications, Mineola, New York, USA, reprint of the John Wiley & Sons, New York, USA, 1982 edition, 1993.

Hansen, A. and Foslien, W.: A macroscale mixture theory analysis of deposition and sublimation rates during heat and mass transfer in dry snow, The Cryosphere, 9, 1857–1878, https://doi.org/10.5194/tc-9-1857-2015, 2015.

Huang, K., Zhang, R., and van Genuchten, M. T.: An Eulerian-Lagrangian approach with an adaptively corrected method of characteristics to simulate variably saturated water flow, Water Resources Research, 30, 499–507, https://doi.org/10.1029/93WR02881, 1994.

Jafari, M., Gouttevin, I., Couttet, M., Wever, N., Michel, A., Sharma, V., Rossmann, L., Maass, N., Nicolaus, M., and Lehning, M.: The Impact of Diffusive Water Vapor Transport on Snow Profiles in Deep and Shallow Snow Covers and on Sea Ice, Frontiers in Earth Science, 8, 249, https://doi.org/10.3389/feart.2020.00249, 2020.

Johnson, J. B.: Snow Deformation, in: Encyclopedia of Earth Sciences Series, pp. 1041–1045, Springer, Dordrecht, Netherlands, https://doi.org/10.1007/978-90-481-2642-2_501, 2011.

Kirchner, H. K., Michot, G., Narita, H., and Suzuki, T.: Snow as a foam of ice: Plasticity, fracture and the brittle-to-ductile transition, Philosophical Magazine A, 81, 2161–2181, https://doi.org/10.1080/01418610108217141, 2001.

Kowalski, J. and Torrilhon, M.: Moment Approximations and Model Cascades for Shallow Flow, Communications in Computational Physics, 25, 669–702, https://doi.org/10.4208/cicp.oa-2017-0263, 2019.

Krinner, G., Derksen, C., Essery, R., Flanner, M., Hagemann, S., Clark, M., Hall, A., Rott, H., Brutel-Vuilmet, C., Kim, H., Ménard, C. B., Mudryk, L., Thackeray, C., Wang, L., Arduini, G., Balsamo, G., Bartlett, P., Boike, J., Boone, A., Chéruy, F., Colin, J., Cuntz, M., Dai,

https://doi.org/10.5194/tc-2021-73
Preprint. Discussion started: 25 March 2021

Y., Decharme, B., Derry, J., Ducharne, A., Dutra, E., Fang, X., Fierz, C., Ghattas, J., Gusev, Y., Haverd, V., Kontu, A., Lafaysse, M., Law, R., Lawrence, D., Li, W., Marke, T., Marks, D., Ménégoz, M., Nasonova, O., Nitta, T., Niwano, M., Pomeroy, J., Raleigh, M. S., Schaedler, G., Semenov, V., Smirnova, T. G., Stacke, T., Strasser, U., Svenson, S., Turkov, D., Wang, T., Wever, N., Yuan, H., Zhou, W., and Zhu, D.: ESM-SnowMIP: assessing snow models and quantifying snow-related climate feedbacks, Geoscientific Model Development, 11, 5027–5049, https://doi.org/10.5194/gmd-11-5027-2018, 2018.

Lacroix, M. and Garon, A.: Numerical Solution of phase change problems: an Eulerian-Lagrangian approach, Numerical Heat Transfer, Part B, 19, 57–78, https://doi.org/10.1080/10407799208944922, 1992.

Lehning, M., Bartelt, P., Brown, B., Fierz, C., and Satyawali, P.: A physical SNOWPACK model for the Swiss avalanche warning: Part II. Snow microstructure, Cold Regions Science and Technology, 35, 147–167, https://doi.org/10.1016/s0165-232x(02)00073-3, 2002.

Libbrecht, K. G.: Physical properties of ice, http://www.cco.caltech.edu/~atomic/snowcrystals/ice/ice.htm, last access: 11 December 2020, 1999.

Lundin, J. M., Stevens, C. M., Arthern, R., Buizert, C., Orsi, A., Ligtenberg, S. R., Simonsen, S. B., Cummings, E., Essery, R., Leahy, W., Harris, P., Helsen, M. M., and Waddington, E. D.: Firn Model Intercomparison Experiment (FirnMICE), Journal of Glaciology, 63, 401–422, https://doi.org/10.1017/jog.2016.114, 2017.

Mellor, G. L. and Blumberg, A. F.: Modeling Vertical and Horizontal Diffusivities with the Sigma Coordinate System, Monthly Weather Review, 113, 1379–1383, https://doi.org/10.1175/1520-0493(1985)113<1379:mvahdw>2.0.co;2, 1985.

Meyer, C. R., Keegan, K. M., Baker, I., and Hawley, R. L.: A model for French-press experiments of dry snow compaction, The Cryosphere, 14, 1449–1458, https://doi.org/10.5194/tc-14-1449-2020, 2020.

Morland, L. W.: A fixed domain method for diffusion with a moving boundary, Journal of Engineering Mathematics, 16, 259–269, https://doi.org/10.1007/bf00042720, 1982.

Paterson, W.: The Physics of Glaciers, Pergamon international library of science, technology, engineering and social studies, Elsevier, 1994.

Schürholt, K., Kowalski, J., and Löwe, H.: Elements of future snowpack modeling - part 1: A physical instability arising from the non-linear coupling of transport and phase changes, companion paper, 2020.

Vionnet, V., Brun, E., Morin, S., Boone, A., Faroux, S., Moigne, P. L., Martin, E., and Willemet, J.-M.: The detailed snowpack scheme Crocus and its implementation in SURFEX v7.2, Geoscientific Model Development, 5, 773–791, https://doi.org/10.5194/gmd-5-773-2012, 2012.

Wever, N., Fierz, C., Mitterer, C., Hirashima, H., and Lehning, M.: Solving Richards Equation for snow improves snowpack meltwater runoff estimations in detailed multi-layer snowpack model, The Cryosphere, 8, 257–274, https://doi.org/10.5194/tc-8-257-2014, 2014.

Wiese, M. and Schneebeli, M.: Early-stage interaction between settlement and temperature-gradient metamorphism, Journal of Glaciology, 63, 652–662, https://doi.org/10.1017/jog.2017.31, 2017.

Wingham, D. J.: Small fluctuations in the density and thickness of a dry firn column, Journal of Glaciology, 46, 399–411, https://doi.org/10.3189/172756500781833089, 2000.